Systems-level overview of host protein phosphorylation during Shigella flexneri infection revealed by phosphoproteomics

Schmutz, Christoph ; Ahrné, Erik ; Kasper, Christoph Alexander ; Tschon, Therese ; Sorg, Isabel ; Dreier, Roland Felix ; Schmidt, Alexander ; Arrieumerlou, Cecile

Abstract: The enteroinvasive bacterium Shigella flexneri invades the intestinal epithelium of humans. During infection, several injected effector proteins promote bacterial internalization, and interfere with multiple host cell responses. To obtain a systems-level overview of host signaling during infection, we analyzed the global dynamics of protein phosphorylation by LC-MS/MS and identified several hundred of proteins undergoing a phosphorylation change during the first hours of infection. Functional bioinformatic analysis revealed that they were mostly related to the cytoskeleton, transcription, signal transduction, and cell cycle. Fuzzy c-means clustering identified six temporal profiles of phosphorylation and a functional module composed of ATM-phosphorylated proteins related to genotoxic stress. Pathway enrichment analysis defined mTOR as the most overrepresented pathway. We showed that mTOR complex 1 and 2 were required for S6 kinase and AKT activation, respectively. Comparison with a published phosphoproteome of Salmonella typhimurium-infected cells revealed a large subset of co-regulated phosphoproteins. Finally, we showed that S. flexneri effector OspF affected the phosphorylation of several hundred proteins, thereby demonstrating the wide-reaching impact of a single bacterial effector on the host signaling network.

DOI: https://doi.org/10.1074/mcp.M113.029918

Systems-level overview of host protein phosphorylation during *Shigella flexneri* infection revealed by phosphoproteomics

Christoph Schmutz, Erik Ahrné, Christoph Alexander Kasper, Therese Tschon, Isabel Sorg, Roland Felix Dreier, Alexander Schmidt and Cécile Arrieumerlou*

Biozentrum, University of Basel, Klingelbergstrasse 50/70, 4056 Basel, Switzerland

Running title: Protein phosphorylation during bacterial infection

*Correspondence:
Prof. Cécile Arrieumerlou
Focal Area Infection Biology
Biozentrum, University of Basel
Klingelbergstrasse 50/70
CH-4056 Basel
Switzerland
Tel.: +41 61 267 21 20
Fax: +41 61 267 21 18
E-mail: cecile.arrieumerlou@unibas.ch

ABBREVIATIONS

Shigella flexneri, S. flexneri; wt, wild-type; interleukin-8, IL-8; Mitogen-activated protein kinase, MAPK; mammalian target of rapamycin, mTOR; liquid chromatography tandem mass spectrometry, LC-MS/MS; Database for Annotation Visualization and Integrated Discovery, DAVID; nuclear pore complex, NPC; mTOR complex 1, mTORC1; mTOR complex 2, mTORC2; regulatory-associated protein of mTOR, Raptor; mammalian LST8/G-protein β-subunit like protein, mLST8/GβL; rapamycin-insensitive companion of mTOR, Rictor; mammalian stress-activated protein kinase interacting protein 1, mSIN1; anaphase-promoting complex/cyclosome, APC/C; inducible Rictor-knockout, iRiKO; mouse embryonic fibroblasts, MEFs; tryptic soy broth, TSB.

ABSTRACT

The enteroinvasive bacterium *Shigella flexneri* invades the intestinal epithelium of humans. During infection, several injected effector proteins promote bacterial internalization, and interfere with multiple host cell responses. To obtain a systems-level overview of host signaling during infection, we analyzed the global dynamics of protein phosphorylation by LC-MS/MS and identified several hundred of proteins undergoing a phosphorylation change during the first hours of infection. Functional bioinformatic analysis revealed that they were mostly related to the cytoskeleton, transcription, signal transduction, and cell cycle. Fuzzy c-means clustering identified six temporal profiles of phosphorylation and a functional module composed of ATM-phosphorylated proteins related to genotoxic stress. Pathway enrichment analysis defined mTOR as the most overrepresented pathway. We showed that mTOR complex 1 and 2 were required for S6 kinase and AKT activation, respectively. Comparison with a published phosphoproteome of *Salmonella typhimurium*-infected cells revealed a large subset of co-regulated phosphoproteins. Finally, we showed that *S. flexneri* effector OspF affected the phosphorylation of several hundred proteins, thereby demonstrating the wide-reaching impact of a single bacterial effector on the host signaling network.

INTRODUCTION

The enteroinvasive bacterium *Shigella flexneri* invades the intestinal epithelium of humans, causing an acute mucosal inflammation called shigellosis or bacillary dysentery that is responsible for 1.1 million deaths annually [1]. During the infectious process, bacteria use a sophisticated delivery system, the type III secretion apparatus, to inject multiple effector proteins that subvert cellular and immune functions of macrophages and epithelial cells [2]. First, *S. flexneri* crosses the colonic epithelium by transcytosis via M cells [3,4]. Released in the M cell pocket, it invades resident macrophages and induces cell death [5,6]. Dying macrophages release bacteria and several proinflammatory cytokines including IL-1β and IL-18 that contribute to acute intestinal inflammation [7,8]. *S. flexneri* is then able to invade epithelial cells via the basolateral surface, and use them as replication niche [9]. Although infection of epithelial cells represents a key aspect of infection, there is currently no comprehensive model that describes the molecular processes occurring in the first hours of infection.

The entry of *S. flexneri* into epithelial cells is a multi-step process that requires the secretion of effector proteins into the cytoplasm of target cells via type III secretion. Upon contact between the tip complex of the type III apparatus and host cell receptors, including α5β1-integrins and CD44, the secreted proteins IpaB and IpaC insert into the plasma membrane and form a pore into the host membrane through which several effectors translocate [10-14]. Among these, IpaA, IpaB, IpaC, IpgB1, IpgB2, IpgD and VirA act synergistically to induce membrane ruffling and bacterial internalization [2]. Local remodeling of the cell surface depends on the interplay between these effectors and small Rho GTPases, kinases and other regulators of the actin cytoskeleton and microtubules [15,16]. Engulfed bacteria rapidly lyse the membrane of their internalization

76 vacuole and escape into the cytoplasm where they multiply, and use actin based motility
77 to spread from cell-to-cell [17]. *Shigella*-actin based motility is mediated by the virulence
78 factor IcsA/VirG [18,19]. This autotransporter, which accumulates at one pole of the
79 bacterium, recruits the host protein N-WASP and forms together with vinculin and
80 Arp2/3, a complex that serves as actin polymerization nucleator [20].

81 Although, epithelial cells are not professional immune cells, they can detect invasion and
82 contribute to acute inflammation by secreting several proinflammatory cytokines such as
83 interleukin-8 (IL-8) and tumor necrosis factor α [21]. During *S. flexneri* infection,
84 peptidoglycan-derived muramyl peptides are recognized via the receptor Nod1 [22]. This
85 recognition leads to the activation of multiple signaling pathways including NF-κB and
86 MAP kinase (MAPK). Bacteria manipulate host signaling in infected cells by secreting
87 effectors that affect different signaling pathways. For instance, the effector OspF, which
88 functions as a phosphothreonine lyase, dephosphorylates MAPKs p38 and ERK in the
89 nucleus of infected cells [23,24]. It was proposed that this mechanism leads to reduced
90 histone H3 phosphorylation and selective repression of gene transcription. Expression of
91 the gene encoding for IL-8, a potent chemoattractant for polymorphonuclear cells, is
92 specifically decreased in presence of OspF. A recent study from our laboratory reported
93 a mechanism of cell-cell communication between infected and uninfected bystander
94 cells that restores IL-8 expression in infected cell monolayers, and potentiates
95 inflammation during infection [25].

96 *S. flexneri* infection of epithelial cells has been well investigated by reductionist
97 approaches that led to important findings regarding specific molecular aspects of
98 infection, and general concepts of infection biology and immunology [26,27]. In addition,

DNA microarrays were instrumental in the systematic identification of genes regulated during infection and the characterization of host cell responses [28,29]. However, these approaches were not well-suited to obtain a systems-level overview of early host signaling during infection.

Protein phosphorylation is the most widespread known post-translational modification. It can either activate or inactivate biological processes, and is commonly used to switch enzyme activity "on" or "off". Protein kinases and phosphatases are abundant in the human genome, giving rise to countless phosphorylation and dephosphorylation events that control the most diverse cellular pathways. Incidentally, the importance of protein phosphorylation has been already described for several aspects of *S. flexneri* infection, and few kinases have been identified [30-33]. Based on this, we reasoned that the complexity of host signaling during *S. flexneri* infection may be addressed by a systematic and unbiased analysis of protein phosphorylation. Here we describe a label-free quantitative phosphoproteomics approach that reveals the dynamics of host protein phosphorylation during infection. Several hundred of proteins undergoing a change in phosphorylation during the first two hours of infection were identified and functionally characterized. Bioinformatic tools were used to recognize six different temporal profiles of phosphorylation, a functional module composed of ATM-phosphorylated proteins related to genotoxic stress, and the central role of mammalian target of rapamycin (mTOR). By comparing our data to a recently published phosphoproteomics analysis of *Salmonella typhimurium* infection [34], we identified a large set of co-regulated phosphoproteins. Finally, we showed that *S. flexneri* effector OspF alters the phosphorylation of several hundred proteins, thereby demonstrating its broad impact during infection.

RESULTS

Label-free quantitative phosphoproteomics reveals the massive impact of *S. flexneri* infection on host protein phosphorylation

To analyze the impact of *S. flexneri* infection on protein phosphorylation in epithelial cells, we used a phosphoproteomics strategy that combines phosphopeptide enrichment and label-free quantification based on liquid chromatography coupled to tandem mass spectrometry (LC-MS/MS) (Figure 1A) [35,36]. In three independent experiments, epithelial cells from the HeLa cell line were left untreated or infected with *S. flexneri* for 15, 30, 60 and 120 minutes at a multiplicity of infection of 40 (Figure 1A). Cell lysis, enzymatic proteolysis, phosphopeptide enrichment on titanium dioxide beads, identification and quantification of individual phosphopeptides were performed as described in Methods. A total of 3234 phosphopeptides corresponding to 3785 phospho-sites and 1184 phosphorylated proteins were identified (Table S1). Analysis of all detected phosphopeptides revealed that the distribution of phosphorylated peptides was strongly biased towards single and dual phosphorylations (Figure 1B, upper panel). As previously described [37], the large majority of phosphorylation events were found on serine and threonine residues (Figure 1B, lower panel). Correlation analysis based on squared Pearson correlation coefficient R^2 between the three biological replicates showed robust reproducibility between independent experiments for all infection conditions (Figure S1A). This was confirmed by data showing that the coefficients of variance calculated for all infection conditions as described in Methods varied between 18% and 29% (Figure S1B), a range of values expected for label-free quantification methods [38,39]. Significant changes in phosphorylation were defined by a q-value (moderated t-test adjusted for multiple testing) cutoff of < 0.01 using the SafeQuant tool

147 [40] and a minimum two-fold increase or decrease in peptide phosphorylation between
148 infected and uninfected control cells (Table S1). Based on these criteria, 14.3% of all
149 detected phosphopeptides showed a significant change in phosphorylation after *S.*
150 *flexneri* infection. A parallel LC-MS/MS analysis, performed before phosphopeptide
151 enrichment (Figure 1A), showed no significant changes in protein amount after infection
152 for significantly altered phosphopeptides (Table S2), demonstrating that changes in
153 phosphopeptide detection reflected true changes in phosphorylation. Phosphorylation
154 events were visible at all time-points with a peak at 30 minutes at which 177
155 phosphopeptides corresponding to 137 phosphorylated proteins showed an increase in
156 phosphorylation compared to control cells (Figure 1C and 1D). Decreased
157 phosphorylation was also detected at all time-points with a maximum of 200 peptides
158 corresponding to 140 proteins showing reduced phosphorylation 2 hours post-infection
159 (Figure 1C and 1D). For simplification, we defined as phosphoproteome the subset of
160 334 proteins undergoing a significant change of phosphorylation on at least one
161 phosphopeptide after infection (Table S1). Previous data showing dual phosphorylation
162 of ERK at residues threonine 202 and tyrosine 204 after *S. flexneri* infection [41] were
163 confirmed by our phosphoproteomics data (Table S1). Taken together, these results
164 showed that *S. flexneri* has a massive impact on host protein phosphorylation, and that
165 label free quantitative phosphoproteomics is well suited to reproducibly identify and
166 quantify the phosphorylation changes occurring during infection of epithelial cells.
167
168 **Phosphoproteomics reveals new cellular functions affected by infection**
169 To analyze the biological functions of proteins with altered phosphorylation during *S.*
170 *flexneri* infection, a gene ontology analysis was performed by using the functional

annotation tool of the Database for Annotation, Visualization and Integrated Discovery (DAVID, http://david.abcc.ncifcrf.gov/) [42,43]. For enrichment analysis, the whole human genome was taken as background. Biases in the calculation of ontology term enrichment were minimized by comparing the 334 proteins of the altered phosphoproteome to a subset of 334 proteins randomly selected among proteins with unchanged phosphorylation (Figure 2A and Table S3). Results showed a strong comparative enrichment in proteins related to cytoskeleton, cell cycle, small GTPases signaling and cell death. In contrast, proteins associated with RNA processing and mRNA splicing were underrepresented in the phosphoproteome. A systematic literature search was performed to refine the functional annotation of gene ontology terms (Figure 2B, Table S4). This analysis revealed that 40 proteins of the phosphoproteome of *S. flexneri*-infected cells were implicated in the organization and rearrangement of the actin cytoskeleton. This included actin-binding proteins that regulate actin polymerization (i.e. ARPC1, PALLD, CTTN), GTP exchange factors (i.e. ARHGEF7, DOCK9, ARHGEF16 and ARHGEF17), GTPase activating proteins (i.e. ARHGAP29, IQGAP2) and downstream effectors (i.e. BORG5) of the small GTPases Cdc42, Rac and RhoA known to be involved in filopodia, membrane ruffling and stress fiber formation, respectively [44,45]. The comparison with the phosphoproteome of cells infected by a deletion virG mutant (Δ*virG*) that cannot perform actin-based motility [19] suggested that proteins undergoing similar phosphorylation changes after both types of infection were important for the cortical actin rearrangements taking place during bacterial internalization (Tables S1 and S5). In contrast, phosphoproteins found exclusively in the wild-type dataset may be either important for actin-based motility or not detected in the LC-MS/MS experiment for technical reasons (Table S5). In addition to proteins regulating the actin cytoskeleton,

proteins associated with the network of microtubules (i.e. MAP1B, MAP7, ELM4) and intermediate filaments (i.e. PLEC, SYNM) were found. These results were expected as it is well documented that *S. flexneri* induces a profound remodeling of actin and microtubules for bacterial uptake and intra- and intercellular motility [2]. In line with data showing that *S. flexneri* interferes with cell-cell adhesion [46], the phosphorylation of proteins involved in the assembly of tight junctions in enterocytes (ZO-1 and ZO-2) and the regulation of adherens junctions (CTNA1, CTND1) was altered in infected cells (Table S4). With around 50 members, proteins implicated in signal transduction were also highly represented in the phosphoproteome. They mainly correspond to receptors, adaptors, kinases and phosphatases involved in well-characterized signaling pathways, including EGFR, MAPK, NF-κB, mTOR and PKA. In addition, 24 proteins related to endocytosis (i.e. SH3GL1, DNMBP), exocytosis (i.e. STXB5) and vesicular trafficking (i.e. BET1, Rab7A, WDR44) were also present in the phosphoproteome (Table S4). In line with previous data showing that *S. flexneri* interferes with host cell cycle [47], we found that infection affected the phosphorylation of regulators of mitotic progression that control spindle dynamics and chromosome separation (i.e. NEK9, BOD1L, PDS5B). To note, the proteins SEPT7 and SEPT9 of the septin family, known to be involved in cytokinesis [48] and more recently, in the formation of septin cages around intracellular bacteria [49,50], were found phosphorylated after *S. flexneri* infection (Table S4). In agreement with data reporting that cell fate is controlled by opposite signals [51], we found that the phosphorylation of both pro- and anti-apoptotic proteins (i.e. PDCD4, BAG3, PAWR) was altered in infected cells. For the first time, our data showed that the phosphorylation of several proteins (Nup98, Nup50, Nu214 and TPR) from the nuclear pore complex (NPC) was modified after infection. NPCs are large multiprotein channels

219 embedded in the nuclear envelope that mediate the transport of macromolecules
220 including proteins and RNA between the cytoplasm and the nucleus of eukaryotic cells.
221 The phosphoproteome was graphically illustrated by combining data from the STRING
222 database that assembles protein networks based on known and predicted protein-
223 protein interactions [52], with a functional description of proteins. Only proteins with at
224 least one connection in STRING were represented (Figure 2C). Data showed a complex
225 network with several distinct functional modules containing highly interconnected nodes.
226 As expected, proteins involved in signal transduction were highly connected with
227 members from other groups, including cytoskeleton and cell adhesion.
228 In order to identify the phosphorylation motifs overrepresented in the phosphoproteome,
229 the Motif-X algorithm [53] was applied to all upregulated phosphopeptides. Six distinctive
230 motif sequences, all phosphorylated on a serine, including the motifs RXRXX*S*, RRX*S*,
231 RXX*S*, *S*P, *S*Q and *S*XE, were extracted (Figure S2). To predict the putative kinases of
232 these motifs, we compared them to those of all known substrates of 107 kinase families
233 [54]. The first three motifs showed striking similarities to substrates of the AGC kinases
234 AKT, PKG/PKA/PKC, RSK and of CamKII (Figure S2). The proline directed *S*P motif can
235 be phosphorylated by MAPK, CDC2 and CDK whereas the *S*Q motif is known to be a
236 substrate of ATM/ATR or DNAPK. Finally, the motif *S*XE remotely resembled a substrate
237 motif of CK2. Although AKT was absent from the phosphoproteome (Table S1), we
238 experimentally confirmed its activation and localization at sites of *S. flexneri* entry
239 (Figure S3A and S3B), as previously reported [55]. The high connectivity of AKT within
240 the STRING graphical representation of the phosphoproteome network suggested that
241 this kinase played a central function during infection (Figure S3C). In particular, AKT
242 was highly connected to proteins associated with the actin cytoskeleton and

apoptosis/survival regulation. Phosphopeptides corresponding to active RSK and ERK were found in the phosphoproteome (Table S1) suggesting that these two kinases may be responsible for the phosphorylation of RXX*S* and *S*P motifs during infection, respectively. In addition, phosphorylation changes at the RRX*S* motif were experimentally confirmed by immunoblotting (Figure S4).

Taken together, these results show that *S. flexneri* infection alters the phosphorylation of a complex network of proteins that are involved in several key aspects of epithelial cell biology. They confirm the large impact of *S. flexneri* infection on the actin cytoskeleton and transcription, and show that numerous proteins related to cell cycle, microtubules, intracellular trafficking and the nuclear pore are also affected during infection.

Spatio-temporal dynamics of protein phosphorylation during *S. flexneri* infection

In order to capture the spatial dynamics of phosphorylation during *S. flexneri* infection, we used the human protein atlas (www.proteinatlas.org) database to analyze the subcellular localization of proteins with altered phosphorylation during infection [56]. With 64% coverage of the phosphoproteome, results showed that phosphorylation changes occurred in proteins localized in the cytoplasm, at the plasma membrane, in the nucleus, at the Golgi apparatus and the endoplasmic reticulum (Figure S5A and S5B). Weak differences were observed over time, indicating for rapid and sustained signaling in different subcellular compartments during infection. Early phosphorylation changes after 15 minutes in the nucleus may result from a fast nuclear translocation of host signaling proteins and/or from a rapid translocation of bacterial effectors to the nucleus of infected cells.

Analysis of the temporal dynamics of individual peptides revealed a large heterogeneity in the patterns of phosphorylation changes after *S. flexneri* infection (Figure S5C). Analysis of all peptides taken individually by fuzzy c-means clustering [57] revealed 6 main profiles (Figure 3A, Table S6). Clusters 1 and 2 corresponded to fast and slow decrease in phosphorylation, respectively. Clusters 3, 4 and 5 corresponded to peptides with fast increase in phosphorylation followed by slow, intermediate and fast decrease, respectively. Cluster 6 grouped peptides showing late phosphorylation with a maximum at 2 hours. A functional analysis indicated that the functional categories were not equally represented in all clusters (Table S6). For instance, proteins associated with the cytoskeleton were overrepresented in clusters 1 and 2. In contrast, proteins involved in the p53 pathway and DNA repair were in majority found in cluster 6. In the same line, the most frequent phospho-motif varied between clusters (Figure 3A). A thorough analysis of cluster 6 revealed that among its 23 members, 15 were phosphorylated on a S̲Q motif. As this motif is the consensus sequence for the major sensor of DNA double-strand breaks ATM [58,59], we checked the activation profile of this kinase after *S. flexneri* infection by monitoring its phosphorylation at serine 1981. As shown in Figure 3B and 3C, an increase of ATM phosphorylation was observed at 30 minutes and phosphorylation was maximal after two hours, suggesting that several cluster 6-proteins were targets of ATM. This hypothesis was validated by showing that the phosphorylation of 11 proteins from this cluster was sensitive to the ATM inhibitor KU-60019 (Figure S6A and S6B, Table S7). More generally, dynamics analysis of all peptides phosphorylated on a S̲Q motif after infection revealed also an earlier profile of phosphorylation (Figure S6C), suggesting that another kinase was implicated. In conclusion, analysis of the dynamics of phosphorylation revealed several temporal profiles of phosphorylation

associated with specific enriched phospho-motifs and distinct functional descriptions. In particular, we identified one group of proteins showing maximal phosphorylation on a *S*Q motif two hours post-infection. As they were functionally associated with the p53 pathway and DNA repair, our results suggest that they are involved in a genotoxic stress response to infection. More broadly, these results illustrate how phosphorylation dynamics and phospho-motif enrichment data combined with functional annotation can be used to identify and characterize the host pathways regulated during bacterial infection.

mTORC1 and mTORC2 control S6 kinase and AKT phosphorylation respectively

The KEGG database was used to identify the overrepresented pathways in the phosphoproteome of *S. flexneri*-infected cells [60,61]. With 7 KEGG-annotated proteins, the mTOR signaling pathway was the most overrepresented pathway (Figure 4A, Table S8). mTOR is a central serine/threonine protein kinase that regulates cell growth and metabolism, autophagy, the actin cytoskeleton, cell proliferation, cell survival, protein synthesis and transcription [62]. It is found as part of two different protein complexes. mTOR complex 1 (mTORC1) is composed of mTOR, regulatory-associated protein of mTOR (Raptor), mammalian LST8/G-protein β-subunit like protein (mLST8/GβL) and the recently identified partners PRAS40 and DEPTOR [63]. This complex functions as a sensor for nutrient, redox balance and energy, and controls protein synthesis. mTOR complex 2 (mTORC2) is composed of mTOR, rapamycin-insensitive companion of mTOR (Rictor), mLST8, DEPTOR and mammalian stress-activated protein kinase interacting protein 1 (mSIN1) [63]. mTORC2 has been shown to function as an important regulator of the actin cytoskeleton [64]. As indicated on the mTOR signaling map (Figure

314 4B), components of both mTOR complexes but also regulators and effectors proteins of
315 mTOR, showed altered phosphorylation after *S. flexneri* infection (Table S1). In order to
316 test the implication of mTORC1 during infection, we monitored the effect of rapamycin
317 on the activation of ribosomal S6 kinase, a protein implicated in protein translation
318 known to be a substrate of mTORC1, and found in the phosphoproteome (Table S1). An
319 antibody that recognizes S6 kinase phosphorylated at threonine 389 was used in an
320 immunoblotting experiment. While a strong activation of S6 kinase was confirmed after
321 infection, a short treatment of rapamycin blocked this induction (Figure 4C, upper panel).
322 The phosphorylation of S6 ribosomal protein, the main substrate of S6 kinase, was also
323 sensitive to rapamycin (Figure 4C, lower panel). In the same condition of drug treatment,
324 rapamycin had no effect on *S. flexneri* entry into cells (Figure 4D). Taken together, these
325 results show that mTORC1 is involved in the early activation of S6 kinase following *S.*
326 *flexneri* infection, and suggest that it may control protein translation.
327 In addition to mTORC1, proteins from the mTORC2 pathway were also found in the
328 phosphoproteome (Figure 4B, Table S1). Although this complex is known to control the
329 actin cytoskeleton, inhibition of mTORC2 had no effect on bacterial invasion (Figure 4C).
330 As AKT was activated during *S. flexneri* infection (Figure S3A and S3B) and is a known
331 substrate of mTORC2, we tested whether mTORC2 played a role in the activation of
332 AKT during infection. Interestingly, AKT phosphorylation was blocked by PP242, an
333 inhibitor of both complexes, but unchanged after rapamycin treatment (Figure 4E),
334 showing that mTORC2 alone was implicated in the activation of AKT during infection.
335 This result was confirmed by showing that AKT phosphorylation was abrogated in
336 inducible Rictor-knockout mouse embryonic fibroblasts [65] treated by tamoxifen (Figure
337 4F). In conclusion, these data show that, mTORC1 controls the phosphorylation of S6

kinase whereas mTORC2 is involved in the activation of AKT. As these two kinases control translation and host cell survival, respectively [55,66,67], our study indicates that mTOR plays a critical role in the control of host cell responses to *S. flexneri* infection.

S. flexneri **and S.** ***typhimurium*** **infections trigger common host phosphorylation changes**

In order to better characterize the phosphoproteome of *S. flexneri*-infected cells, we compared it to a recently published phosphoproteome dataset generated from HeLa cells infected by *Salmonella typhimurium* [34]. This bacterium is also an enteroinvasive pathogen that uses type III secretion to inject multiple effector proteins that facilitate its internalization. However, in contrast to *S. flexneri*, *S. typhimurium* remains enclosed in a vacuole where it replicates. Although different quantitative phosphoproteomics methods were employed, the comparison between the phosphoproteomes of cells infected by *S. flexneri* or *S. typhimurium* showed an overlap of 62 phosphopeptides corresponding to 57 phosphoproteins (Figure 5A, Table 9). Hierarchical clustering and correlation analysis performed on shared phosphopeptides showed a strong correlation of phosphorylation changes with 61 phosphopeptides co-regulated after both infections (Figure S7A and S7B). As expected, proteins involved in the actin cytoskeleton, microtubules, cell-cell adhesion, cell cycle or gene regulation were similarly regulated during infection by both pathogens (Figure 5B). Taken together, these results identify new common molecular processes triggered by *S. flexneri* and *S. typhimurium* in infected epithelial cells, and provide the first large-scale comparison of host signaling after infection by different bacteria.

OspF has a wide-reaching impact on host protein phosphorylation

During infection, *S. flexneri* injects several type III effectors that manipulate the signaling pathways controlling the inflammatory response of infected cells. Several mechanisms of action have been characterized based on the enzymatic activity, the structure or the intracellular binding partners of these effectors. For instance, the effector OspF attenuates IL-8 expression via its phosphothreonine lyase activity that irreversibly dephosphorylates MAPKs p38 and ERK on a T-X-Y motif, thereby preventing downstream histone H3 phosphorylation [23]. We experimentally confirmed that p38 and ERK phosphorylation was restored when cells were infected with a deletion mutant of OspF (Δ*ospF*) compared to wild-type-infected cells (Figure 6A). Interestingly, we found that OspF interfered also with the phosphorylation of the kinase RIP2 and the transcription factor CREB (Figure 6A), two proteins involved in the control of inflammation [68,69], suggesting that OspF had a more complex effect on host signaling than expected. To evaluate its impact, the phosphoproteome of HeLa cells infected by Δ*ospF S. flexneri* was determined by LC-MS/MS. When we directly compared the phosphorylation changes triggered by Δ*ospF* versus wild-type infection (differential phosphoproteome) by hierarchical clustering, we found 377 peptides with increased phosphorylation and 86 with decreased phosphorylation (Table S10 and Figure 6B), showing that OspF had a massive net negative impact on phosphorylation. As expected, phosphoproteomics data confirmed that OspF strongly dephosphorylated ERK and p38 at residues T202/Y204 and T180/Y182, respectively (Table S10). A systematic search for the T-X-Y motif, known to be the consensus motif for the OspF phosphothreonine lyase activity [70], identified GSK3A as a potential new target. To test this hypothesis, we tested whether a treatment with the ERK and p38 inhibitors, PD98059 and

386 SB203580 respectively, abolished all OspF-dependent phosphorylation changes (Table
387 S10). With a q value <0.01 and a minimum 2 fold-ratio, none of the phosphopeptides
388 differentially regulated by OspF (Figure S8A) remained significantly different from wild-
389 type infection after pretreatment with MAPK inhibitors (Figure S8B). In particular,
390 PD98059 and SB203580 completely abolished GSK3A phosphorylation at T201 and
391 Y203 (Figure S8B), indicating that this protein was not a direct substrate of OspF and
392 that this effector affected protein phosphorylation exclusively via its phosphothreonine
393 lyase activity towards ERK and p38. However, because a q-value <0.01 corresponds to
394 a very stringent cutoff, we reasoned that the method employed was likely
395 underestimating the chance to identify inhibitor-insensitive phosphopeptides. Therefore,
396 phosphopeptides with a q-value <0.1 were then considered and sensitivity to the
397 inhibitors was directly tested for one of them. The NPC protein, Nup50, for which a
398 phospho-specific antibody was available, was selected. Its phosphorylation at serine 221
399 was addressed by immunofluorescence. As expected, wild-type and Δ*ospF* bacteria
400 induced a moderate and strong increase of Nup50 phosphorylation, respectively (Figure
401 S9A). Surprisingly, MAPK inhibitors failed to affect Nup50 phosphorylation in cells
402 infected by Δ*ospF* (Figure S9B). This result showed that, although most OspF-
403 dependent phosphorylation changes were sensitive to MAPK inhibitors, the
404 phosphorylation of at least one protein was independent of ERK and p38. Taken
405 together, these data indicate that p38 and ERK are the main targets of OspF, but
406 suggest also that additional proteins may be directly affected by its phosphothreonine
407 lyse activity.
408 A STRING network representation of the differential phosphoproteome showed a core
409 network of 136 proteins connected at least once (Figure 6C). Some of these have direct

410 or indirect connections to ERK and p38. A systematic search for the overrepresented
411 phosphorylation motifs identified among others the *S*P/*T*P motif shared by the MAPKs,
412 Cdc2 and Cdks as well as RXX*S*, which can be phosphorylated by RSK, a kinase
413 identified in the differential phosphoproteome (Figure 6C, Figure S10).
414 It has been shown that OspF interferes with IL-8 expression in *S. flexneri*-infected cells
415 [23]. To further characterize the role of this effector during infection, we analyzed the
416 biological functions of the differential phosphoproteome (Figure 6C and 6D, Table S11).
417 In line with an inhibition of gene expression [23], many proteins involved in transcription,
418 chromatin modification and RNA processing were affected by OspF. Phosphorylation
419 changes in several NPC proteins were also observed. In addition, phosphoproteins
420 related to various biological functions including actin cytoskeleton, microtubules,
421 apoptosis and cell cycle were also affected by OspF (Figure 6D). Altogether, these
422 results show that OspF has a massive impact on host protein phosphorylation and
423 illustrate that, by targeting the central hubs p38 and ERK, this effector shuts down a
424 large fraction of the cellular network.
425

DISCUSSION

For the first time, we used phosphoproteomics to address the dynamics of protein phosphorylation during the first two hours of *S. flexneri* infection in epithelial cells. Using a label-free LC-MS/MS-based approach, we found more than three hundred proteins undergoing a significant change in phosphorylation after infection. This corresponded to 28% of all detected phosphoproteins, showing that infection by the enteroinvasive bacterium *S. flexneri* has a massive impact on host protein phosphorylation. Although label-free LC-MS/MS is not a comprehensive method, our study covered a large portion of the phosphoprotein space and was well-suited to reproducibly identify and quantify host phosphorylation changes after bacterial infection.

Gene ontology analysis and manual functional annotation of the phosphoproteome confirmed the importance of the actin cytoskeleton and microtubules during infection. This result was expected because the first two hours of infection cover the entry mechanism of *S. flexneri* and actin based-motility, two processes highly dependent on actin and microtubule remodeling and controlled by protein phosphorylation [33,71]. The identification of around 50 new phosphoproteins related to the cytoskeleton and the comparison between wild-type and Δ*virG* infection open a new avenue to elucidate the mechanisms of bacterial entry and actin-based motility, two critical processes that contribute to successful colonization of the intestinal epithelium in humans.

Further functional analysis of the phosphoproteome showed that the phosphorylation of proteins related to cell cycle was affected by infection. This result was consistent with a report by Iwai et al. showing that the secreted effector IpaB causes cell-cycle arrest of epithelial cells by targeting Mad2L2, an anaphase-promoting complex/cyclosome (APC/C) inhibitor [47]. The addition of Mad2L2 to the STRING network representation of

450 the phosphoproteome shows that this protein interconnects with CDC23 and BUB1,
451 component and substrate of APC/C respectively, that are important for cell cycle
452 checkpoint enforcement. Interestingly, phosphoproteomics revealed that *S. flexneri*
453 infection alters the phosphorylation of NPC proteins including Nup98, Nup50, Nu214 and
454 TPR. NPCs are composed of around 30 different nucleoporins divided into scaffolding
455 proteins that are important for nuclear pore assembly and maintenance, and peripheral
456 proteins that function directly in nucleo-cytoplasmic transport. Noticeably, all proteins
457 affected by *S. flexneri* infection belong to this second class. Follow up work is required to
458 elucidate how infection impacts nuclear transport, and if trafficking of important host
459 proteins or mRNA is affected during infection. Besides transport, recent studies indicate
460 that peripheral proteins of NPCs can also directly contribute to gene regulation by
461 interacting with chromatin and coupling transcription with mRNA export [72]. It would be
462 of particular interest to investigate whether changes in NPC protein phosphorylation can
463 affect the expression of proinflammatory genes by this mechanism.

464 To better understand the host phosphorylation dynamics of *S. flexneri* infection and
465 extract useful information regarding the roles of functional modules during infection, we
466 used fuzzy c-means clustering to group all individual phosphopeptide based on the
467 direction and the temporal profiles of phosphorylation changes after infection. Each
468 cluster was then analyzed for the most frequent phospho-motifs and functional
469 annotation of proteins. For clusters showing a fast (cluster 1) or slow reduction (cluster2)
470 of phosphorylation, the <u>*S*</u>P phospho-motif was highly enriched. As this motif can be
471 phosphorylated by MAPKs, we hypothesize that, for some proteins, the reduction of
472 phosphorylation results from the phosphothreonine lyase activity of OspF on p38 and
473 ERK. Alternatively, a reduction of <u>*S*</u>P phosphorylation can also be explained by the

474 inhibition of other kinases like CDC2 and CDK. In a non-exclusive manner, the activation
475 of phosphatases may also play a role. Remarkably, proteins from cluster 1 were in
476 majority involved in the regulation of the actin cytoskeleton, microtubules and cell
477 adhesion. In contrast, proteins belonging to cluster 2 were essentially related to
478 transcription. Among the other profiles of phosphorylation changes, cluster 6 showed
479 maximal phosphorylation two hours post-infection. For this cluster, 14 proteins out of 21
480 were phosphorylated on an *S*Q motif, a known substrate of ATM, ATR and DNAPK. By
481 monitoring the activation of ATM at different time-points of infection by immunoblotting,
482 we observed a very similar kinetics of activation, suggesting that ATM phosphorylated
483 the *S*Q-containing proteins of cluster 6. This hypothesis was confirmed by showing that
484 the ATM inhibitor KU60019 inhibited the phosphorylation of most of them. As these
485 proteins were strongly associated with the p53 pathway and DNA repair, we propose
486 that they belong to a functional module related to genotoxic stress. This assumption is
487 supported by a recent article reporting *S. flexneri*-induced genotoxic stress and ATM
488 activation [73].

489 Finally, in the clusters showing an increase in phosphorylation, the *S*P and RXX*S*
490 phospho-motifs were overrepresented. The latter can be phosphorylated by AGC
491 kinases such as AKT, PKA, PKC, S6 kinase and the members of the RSK family.
492 Whereas our phosphoproteomics data supported the activation of S6 kinase and RSK
493 during infection, phosphorylated AKT was not detected. By using an antibody that
494 recognizes the active form of AKT, we confirmed its activation after *S. flexneri* infection
495 and localization at entry foci. Although it was reported that AKT activation requires an
496 IpgD-dependent production of phosphatidylinositol 5 monophosphate [55] and EGF
497 receptor signaling [74], its exact mechanism of activation remains unclear. Here we

found that AKT activation was sensitive to PP242 but not to rapamycin, and was abolished in cells depleted of Rictor, showing clearly that AKT activation was dependent on mTORC2. The implication of mTORC2 was also supported by the phosphoproteomics data showing that both mSin1 and Rictor underwent a change in phosphorylation during *S. flexneri* infection. Further experiments are required to test how mTORC2 is activated during infection. Because AKT controls the survival of infected cells [55,67], our data indicated that mTORC2 was involved in the regulation of cell fate during infection. Interestingly, although mTORC2 can regulate the actin cytoskeleton [64], bacterial entry was not affected by the inhibition of mTORC2. In addition, phosphoproteomics revealed a rapid change in phosphorylation for the two mTORC1 components Raptor and PRAS40, indicating that mTORC1 was implicated in the early phase of infection. This finding was supported by the observation that the phosphorylation of S6 kinase and S6 ribosomal protein observed 15 minutes post infection was sensitive to rapamycin and PP242 treatment. Because these two proteins are known to regulate protein translation, these results suggested that mTORC1 participates to the control of host protein synthesis during *S. flexneri* infection. Interestingly, a recent report by Tattoli et al. shows that *S. flexneri* infection leads to amino acid starvation and to a subsequent down-regulation of mTORC1 activity that induces autophagy [75]. The authors report that amino acid starvation is sensed by GCN2 which becomes phosphorylated within the first hour of infection. Altogether, these two studies support the roles of both mTORC1 and mTORC2, and identify mTOR as a central host player of *S. flexneri* infection.

Phosphoproteomics is a method that has been applied only recently to the field of bacterial infection with a first study by Rogers et al. investigating *S. typhimurium*

infection of epithelial cells [34]. As *S. flexneri* and *S. typhimurium* are closely related and both harbor a type III secretion system with several homologue effectors, we compared the respective phosphoproteomes of infected HeLa cells. Although major differences in sample preparation and phosphoproteomics methodology exist between the two studies [76], 61 co-regulated phosphopeptides were discovered. These results demonstrated that *S. flexneri* and *S. typhimurium* induce various common host molecular processes in infected cells. Among the shared phosphopeptides, many belong to proteins related to the cytoskeleton and its regulation. For instance, the protein palladin, strongly phosphorylated after *S. flexneri* and *S. typhimurium* infection, is known to localize at sites of actin remodeling including ruffles and lamellipodia. The protein IQGAP2 interacts with CDC42 and Rac1, two GTPases required for efficient bacterial entry [77,78]. Taken together, these data constitute the first large-scale comparison of host signaling after infection by different pathogenic bacteria. By identifying the common phosphorylation events, this approach allows to define the host pathways that are co-regulated by pathogens, and may facilitate the identification of processes that could be targeted by broad-spectrum drugs in the perspective of treatments against bacterial infections.

As previously described, *S. flexneri* secretes different effectors that manipulate host signaling to finely tune the inflammatory response of infected cells. For instance, it was proposed that OspF blocks the expression of IL-8 by altering the phosphorylation of histone H3 and the access of transcription factors to chromatin [23]. Phosphoproteomics revealed that OspF affects the phosphorylation of more than three hundred proteins, showing that this effector has a wider impact than anticipated. The MAPK inhibitors, PD98059 and SB203580, abolished almost all OspF-dependent phosphorylation changes, suggesting that they resulted from its phosphothreonine lyase activity towards

546 p38 and ERK. However, the observation that, Nup50 phosphorylation was not sensitive
547 to MAPK inhibitors, suggests that OspF targets additional proteins. In line with an effect
548 of OspF on gene regulation, the phosphorylation of various proteins associated with
549 transcription, chromatin modification and RNA processing was strongly affected.
550 However, the biological functions and the number of proteins impacted by OspF strongly
551 suggested that a reduction of histone H3 phosphorylation was not the only mechanism
552 by which the effector OspF affected IL-8 expression in infected cells. Further functional
553 analysis revealed that phosphoproteins associated with the actin cytoskeleton,
554 microtubules, cell cycle and intracellular transport were also altered by OspF. Altogether,
555 these results illustrate how *S. flexneri* effectively alters a large fraction of the host protein
556 phosphorylation network via a single effector. They also demonstrate that OspF can be
557 used as a molecular tool to discover new targets of MAPKs, and decipher novel
558 downstream regulatory mechanisms.

559 In summary, we used quantitative phosphoproteomics to investigate host signaling
560 during *S. flexneri* infection of epithelial cells. We found several hundred of proteins
561 undergoing a significant change in phosphorylation during the first two hours of infection.
562 Dynamics studies combined with functional annotation and phospho-motif enrichment
563 demonstrated alterations of proteins involved in different cellular functions, including the
564 cytoskeleton, cell cycle, transcription, and genotoxic stress responses. In addition, we
565 discovered an early signaling function of mTOR during infection, and characterized the
566 impact of OspF on host protein phosphorylation. In conclusion, these data provide the
567 first systems-level overview of host signaling during the first hours of a bacterial
568 infection, and constitute a valuable resource for generating testable hypotheses related
569 to host-pathogen interactions.

METHODS

Reagents and antibodies

PP242 was obtained from Chemdea (#CD0258), Rapamycin from LC Laboratories (#R-5000), KU-60019 (#S1570), SB203580 (#S1076) and PD98059 (#S1177) from Selleck chemicals. Antibodies against MAPK p38 (#9212), phospho-MAPK p38 Thr180/Tyr182 (#4631), ERK (#9102), pospho-ERK (Thr202/Tyr204) (#4377), RIP2 (#4982), phospho-RIP2 Ser176 (#4364), CREB (#9197), phospho-CREB Ser133 (#9198), phospho-AKT Ser473 (#4058), phospho-ATM Ser1981 (#5883), phospho-S6 ribosomal protein Ser235/Ser236 (#4858), phospho-S6K Thr389 (#9205) and Rictor (#2114) were obtained from Cell Signaling Technology. Antibodies against ATM (#05-513) and actin (#MAB1501) were purchased from Millipore. The antibody against vinculin was purchased from Sigma (#V9131). The antibody against NUP50 phosphorylated at Ser221 was kindly provided by Prof. H. Kosako (Tokushima University, Japan).

Cell culture

HeLa CCL-2™ cells were purchased from ATCC and cultured in DMEM, supplemented with 10% FCS, antibiotics and L-glutamine. Inducible Rictor-knockout (iRiKO) mouse embryonic fibroblasts (MEFs) and the corresponding control cells were generously provided by Prof. M. Hall [65]. MEFs were cultured in DMEM, supplemented with 10% FCS, antibiotics and L-glutamine. The knockout of Rictor was induced by culturing the cells for three days in the presence of 1μM Tamoxifen.

Bacterial strains

593 The M90T *S. flexneri* and M90T *S. flexneri* Δ*virG* strains were generously provided by
594 Prof. P. Sansonetti (Institut Pasteur, Paris, France). The *ospF* deletion mutant (Δ*ospF*)
595 was generated by allelic exchange using a modification of the lambda red-mediated
596 gene deletion as previously described [79]. *S. flexneri* M90T Δ*virG* pCK100
597 (P_{uhpT}::DsRed) was generated by transforming the non-motile *S. flexneri* strain M90T
598 Δ*virG* with the plasmid pCK100. pCK100 contains the fluorescent marker DsRed under
599 the control of the native promoter of the *S. flexneri* gene *uhpT*, which is upregulated in
600 presence of glucose-6-phosphate. Briefly, the 251bp promoter region upstream of *uhpT*
601 was amplified by PCR (Primers used:
602 GAGAGAGAATGCAGTGCTCGATACCTGGCACT, GCTCTAGAGGGTTACTCCTGAAA
603 TGAATACCT) and ligated into the pMW211 plasmid using *Bsm*I and *Xba*I.

604

605 **Infection assay**

606 M90T *S. flexneri* strain was grown in tryptic soy broth (TSB) to exponential growth phase
607 at 37°C and coated with poly-L-lysine. 30 minutes before infection, complete growth
608 medium was replaced by DMEM supplemented with 10 mM Hepes and 2 mM L-
609 glutamine (assay medium). Assay medium (uninfected control) or bacteria were added
610 to 6-well plates at a multiplicity of infection of 40. Infection was initiated by centrifugation
611 of the plates for 5 minutes and their incubation at 37°C for the indicated time periods.
612 Extracellular bacteria were killed by adding gentamycin (50 µg/ml) 30 minutes after
613 infection.

614

615 **Microscopy and automated image analysis**

Infection rates were determined by using automated image analysis. Images were automatically acquired with an ImageXpress Micro (Molecular devices, Sunnyvale, USA). At each site, images were acquired at 360 nm, 480 nm, 594 nm and 640 nm to visualize Hoechst, FITC-phalloidin, DsRed-expressing *S. flexneri* and Alexa 647-conjugated secondary antibodies, respectively. Infection rates were determined by image analysis using CellProfiler [80] and MATLAB (The MathWorks, Inc, Natick, USA). The Hoechst staining was used as a mask to automatically identify cell nuclei. The cellular area was defined by extension of the nuclear mask. In parallel, the presence of bacteria within the area of each cell was quantified. Performance of bacterial detection was checked by visual inspection of several images prior to automated processing. In control images (no infection), the algorithm generally classified less than 1% of cells as infected [25].

SDS-PAGE and immunoblotting

Uninfected control and infected cells were washed twice in ice cold PBS, lysed in PhosphoSafe™ extraction reagent (Novagen), incubated on ice for 10 minutes, and subsequently centrifuged at 4°C for 20 minutes at 16'000g. BCA Protein Assay kit (Pierce) was used to determine protein concentration. 10-15 μg of protein was subjected to SDS-polyacrylamide gels and electroblotted onto nitrocellulose membranes. Immunoblotting was performed using primary antibodies diluted in phosphate buffered saline containing 0.1% tween and 5% bovine serum albumin. HRP-conjugated secondary antibodies were purchased from GE Healthcare or Cell signaling technology. The blots were developed with an enhanced chemiluminescence method (ECL, Pierce).

Immunofluorescence

After fixation in 4% PFA for 10 minutes, cells were permeabilized in 0.3-0.5% Triton X-100 for 10 minutes. Phospho-AKT antibody was incubated overnight at 4°C in PBS followed by a secondary staining using Alexa 647-conjugated secondary antibody (Invitrogen). Additionally, DNA and F-actin were stained for 1 hour at room temperature with Hoechst and FITC-phalloidin (Invitrogen), respectively.

Sample preparation for phosphoproteomics

For each condition, two 6-well plates of HeLa CCL-2^{TM} cells were grown to confluency. Cells were infected as described above. At the indicated time-points, the plates were put on ice and washed twice with ice-cold phosphate-buffered saline (PBS). Samples were then collected in urea solution [8M Urea (AppliChem), 0.1M Ammoniumbicarbonate (Sigma), 0.1% RapiGest (Waters), 1x PhosSTOP (Roche)]. The samples were briefly vortexed, sonicated at 4°C (Hielscher), shaked for 5 minutes on a thermomixer (Eppendorf) and centrifuged for 20 minutes at 4°C and 16'000g. Supernatants were collected and stored at -80°C for further processing. BCA Protein Assay (Pierce) was used to measure protein concentration.

Phosphopeptide enrichment

Disulfide bonds were reduced with tris(2-carboxyethyl)phosphine at a final concentration of 10 mM at 37°C for 1 hour. Free thiols were alkylated with 20 mM iodoacetamide (Sigma) at room temperature for 30 minutes in the dark. The excess of iodoacetamide was quenched with N-acetyl cysteine at a final concentration of 25 mM for 10 minutes at room temperature. Lys-C endopeptidase (Wako) was added to a final enzyme/protein

ratio of 1:200 (w/w) and incubated for 4 hours at 37°C. The solution was subsequently diluted with 0.1 M ammoniumbicarbonate (Sigma) to a final concentration below 2 M urea and digested overnight at 37°C with sequencing-grade modified trypsin (Promega) at a protein-to-enzyme ratio of 50:1. Peptides were desalted on a C18 Sep-Pak cartridge (Waters) and dried under vacuum. Phosphopeptides were isolated from 2 mg of total peptide mass with TiO_2 as described previously [35]. Briefly, dried peptides were dissolved in an 80% acetonitrile (ACN)–2.5% trifluoroacetic acid (TFA) solution saturated with phthalic acid. Peptides were added to the same amount of equilibrated TiO_2 (5-µm bead size, GL Science) in a blocked Mobicol spin column (MoBiTec) that was incubated for 30 minutes with end-over-end rotation. The column was washed twice with the saturated phthalic acid solution, twice with 80% ACN and 0.1% TFA, and finally twice with 0.1% TFA. The peptides were eluted with a 0.3 M NH_4OH solution. The pH of the eluates was adjusted to be below 2.5 with 5% TFA solution and 2 M HCl. Phosphopeptides were again desalted with microspin C18 cartridges (Harvard Apparatus).

LC-MS/MS analysis

Chromatographic separation of peptides was carried out using an EASY nano-LC system (Thermo Fisher Scientific), equipped with a heated RP-HPLC column (75 µm x 37 cm) packed in-house with 3 µm C18 resin (Reprosil-AQ Pur, Dr. Maisch). Aliquots of 1 µg total phosphopeptide sample were analyzed per LC-MS/MS run using a linear gradient ranging from 98% solvent A (0.15% formic acid) and 2% solvent B (98% acetonitrile, 2% water, 0.15% formic acid) to 30% solvent B over 90 minutes at a flow rate of 200 nl/min. Mass spectrometry analysis was performed on a dual pressure LTQ-

688 Orbitrap mass spectrometer equipped with a nanoelectrospray ion source (both Thermo
689 Fisher Scientific). Each MS1 scan (acquired in the Orbitrap) was followed by collision-
690 induced dissociation (CID, acquired in the LTQ) of the 10 most abundant precursor ions
691 with dynamic exclusion for 30 seconds with enabled multistage activation. Total cycle
692 time was approximately 2 s. For MS1, 10^6 ions were accumulated in the Orbitrap cell
693 over a maximum time of 300 ms and scanned at a resolution of 60,000 FWHM (at 400
694 m/z). MS2 scans were acquired using the normal scan mode, a target setting of 10^4
695 ions, and accumulation time of 50 ms. Singly charged ions and ions with unassigned
696 charge state were excluded from triggering MS2 events. The normalized collision energy
697 was set to 32%, and one microscan was acquired for each spectrum.
698

699 **Label-free quantification and database searching**

700 The acquired raw-files were imported into the Progenesis software tool (Nonlinear
701 Dynamics, Version 4.0) for label-free quantification using the default parameters. MS2
702 spectra were exported directly from Progenesis in mgf format and searched using the
703 MASCOT algorithm (Matrix Science, Version 2.4) against a decoy database [81]
704 containing normal and reverse sequences of the predicted SwissProt entries of *Homo*
705 *sapiens* (www.ebi.ac.uk, release date 16/05/2012) and commonly observed
706 contaminants (in total 41,250 sequences) generated using the SequenceReverser tool
707 from the MaxQuant software (Version 1.0.13.13) . To identify proteins originating from *S.*
708 *flexneri*, non phosphopeptide enriched samples were searched against the same
709 database above including predicted SwissProt entries of *S. flexneri* (www.ebi.ac.uk,
710 release date 16/05/2012, in total 49,610 sequences) The precursor ion tolerance was
711 set to 10 ppm and fragment ion tolerance was set to 0.6 Da. The search criteria were set

712 as follows: full tryptic specificity was required (cleavage after lysine or arginine residues
713 unless followed by proline), 2 missed cleavages were allowed, carbamidomethylation
714 (C) was set as fixed modification and phosphorylation (S,T,Y) or oxidation (M) as a
715 variable modification for TiO2 enriched or not enriched samples, respectively. Finally,
716 the database search results were exported as a xml-file and imported back to the
717 Progenesis software for MS1 feature assignment. For phosphopeptide quantification, a
718 csv-file containing the MS1 peak abundances of all detected features was exported and
719 for not enriched samples, a csv-file containing all protein measurements based on the
720 summed feature intensities of all identified peptides per protein was created. Importantly,
721 the Progenesis software was set that proteins identified by similar sets of peptides are
722 grouped together and that only non-conflicting peptides with specific sequences for
723 single proteins in the database were employed for protein quantification. Both files were
724 further processed using the in-house developed SafeQuant v1.0 R script (unpublished
725 data, available at https://github.com/eahrne/SafeQuant/). In brief, the software sets the
726 identification level False Discovery Rate to 1% (based on the number of decoy protein
727 sequence database hits) and normalizes the identified MS1 peak abundances across all
728 samples. Next, all quantified phosphopeptides/proteins are assigned an abundance ratio
729 and a q-value, per time point. Q-values reflect the quantification level False Discovery
730 Rate of a given ratio cutoff, and are obtained by calculating modified t-statistic p-values
731 [82] and adjusting for multiple testing [83]. The final list of all quantified
732 phosphopeptides/proteins is presented in Table S1/S2. The location of the
733 phosphorylated residues was automatically assigned by MASCOT (score >10). All
734 annotated spectra can be found in supplemental information file 12 (annotated spectra)
735 and, together with the MS raw files and search parameters employed, have been

736 deposited to the ProteomeXchange Consortium
737 (http://proteomecentral.proteomexchange.org) via the PRIDE partner repository [84]
738 (data submitted).
739
740

ACKNOWLEDGEMENTS

We thank Prof. Mike Hall (Biozentrum, University of Basel) for the use of inducible rictor-knockout mouse embryonic fibroblasts, Dr. Timo Glatter for advice regarding LC-MS/MS sample preparation and data analysis, Dr. Lukas Herwig for the acquisition of confocal images and Dr. Simon Ittig for critical reading of the manuscript. This work was funded by the Swiss National Science Foundation (grant 310030-138377/1 to C.A.) and the InfectX and BattleX projects from SystemsX.ch.

AUTHOR CONTRIBUTIONS

Conceived and designed the experiments: CS, CA, AS. Performed the experiments: CS, IS, TT, RD. Analyzed the data: CS, AS, EA, CA, CK. Contributed materials/analysis tools: AS, EA, CK. Wrote the paper: CA, CS.

CONFLICT OF INTEREST

The authors declare that they have no conflict of interest.

REFERENCES

1. Kotloff KL, Winickoff JP, Ivanoff B, Clemens JD, Swerdlow DL, et al. (1999) Global burden of Shigella infections: implications for vaccine development and implementation of control strategies. Bull World Health Organ 77 651-666

2. Schroeder GN, Hilbi H (2008) Molecular Pathogenesis of Shigella spp.: Controlling Host Cell Signaling, Invasion, and Death by Type III Secretion. Clin Microbiol Rev 21: 134-156.

3. Sansonetti PJ, Arondel J, Cantey JR, Prévost MC, Huerre M (1996) Infection of rabbit Peyer's patches by Shigella flexneri: effect of adhesive or invasive bacterial phenotypes on follicle-associated epithelium. Infect Immun 64: 2752-2764.

4. Wassef JS, Keren DF, Mailloux JL (1989) Role of M cells in initial antigen uptake and in ulcer formation in the rabbit intestinal loop model of shigellosis. Infect Immun 57: 858-863.

5. Nonaka T, Kuwabara T, Mimuro H, Kuwae A, Imajoh-Ohmi S (2003) Shigella-induced necrosis and apoptosis of U937 cells and J774 macrophages. Microbiology 149: 2513-2527.

6. Zychlinsky A, Prevost MC, Sansonetti PJ (1992) Shigella flexneri induces apoptosis in infected macrophages. Nature 358: 167-169.

7. Sansonetti PJ, Phalipon A, Arondel J, Thirumalai K, Banerjee S, et al. (2000) Caspase-1 Activation of IL-1β and IL-18 Are Essential for Shigella flexneri–Induced Inflammation. Immunity 12: 581-590.

8. Zychlinsky A, Fitting C, Cavaillon JM, Sansonetti PJ (1994) Interleukin 1 is released by murine macrophages during apoptosis induced by Shigella flexneri. J Clin Invest 94: 1328-1332.

781 9. Mounier J, Vasselon T, Hellio R, Lesourd M, Sansonetti PJ (1992) Shigella flexneri
782 enters human colonic Caco-2 epithelial cells through the basolateral pole. Infect
783 Immun 60: 237-248.
784 10. Blocker A, Gounon P, Larquet E, Niebuhr K, Cabiaux V, et al. (1999) The Tripartite
785 Type III Secreton of Shigella flexneri Inserts Ipab and Ipac into Host Membranes. J
786 Cell Biol 147: 683-693.
787 11. Parsot C (2009) Shigella type III secretion effectors: how, where, when, for what
788 purposes? Curr Opin Microbiol 12: 110-116.
789 12. Frank Lafont GTVN, Kentaro Hanada, Philippe Sansonetti, and F.Gisou van der
790 Goot (2002) Initial steps of Shigella infection depend on the cholesterol/sphingolipid
791 raft-mediated CD44–IpaB interaction. EMBO J 21: 4449-4457.
792 13. Watarai M FS, Sasakawa C. (1996) Interaction of Ipa proteins of Shigella flexneri
793 with alpha5beta1 integrin promotes entry of the bacteria into mammalian cells. J
794 Exp Med 183: 991-999.
795 14. Skoudy A, Mounier J, Aruffo A, Ohayon H, Gounon P, et al. (2000) CD44 binds to
796 the Shigella IpaB protein and participates in bacterial invasion of epithelial cells. Cell
797 Microbiol 2: 19-33.
798 15. Boquet P, Lemichez E (2003) Bacterial virulence factors targeting Rho GTPases:
799 parasitism or symbiosis? Trends Cell Biol 13: 238-246.
800 16. Mounier J, Laurent V, Hall A, Fort P, Carlier MF, et al. (1999) Rho family GTPases
801 control entry of Shigella flexneri into epithelial cells but not intracellular motility. J
802 Cell Sci 112: 2069-2080.

803 17. Sansonetti PJ, Ryter A, Clerc P, Maurelli AT, Mounier J (1986) Multiplication of
804 Shigella flexneri within HeLa cells: lysis of the phagocytic vacuole and plasmid-
805 mediated contact hemolysis. Infect Immun 51: 461-469.
806 18. Bernardini ML, Mounier J, d'Hauteville H, Coquis-Rondon M, Sansonetti PJ (1989)
807 Identification of icsA, a plasmid locus of Shigella flexneri that governs bacterial intra-
808 and intercellular spread through interaction with F-actin. Proc Natl Acad Sci U S A
809 86: 3867-3871.
810 19. Goldberg MB, Theriot JA (1995) Shigella flexneri surface protein IcsA is sufficient to
811 direct actin-based motility. Proc Natl Acad Sci U S A 92: 6572-6576.
812 20. Egile C, Loisel TP, Laurent V, Li R, Pantaloni D, et al. (1999) Activation of the Cdc42
813 Effector N-Wasp by the Shigella flexneri Icsa Protein Promotes Actin Nucleation by
814 Arp2/3 Complex and Bacterial Actin-Based Motility. J Cell Biol 146: 1319-1332.
815 21. Sansonetti PJ, Arondel J, Huerre M, Harada A, Matsushima K (1999) Interleukin-8
816 Controls Bacterial Transepithelial Translocation at the Cost of Epithelial Destruction
817 in Experimental Shigellosis. Infect Immun 67: 1471-1480.
818 22. Girardin SE, Boneca IG, Carneiro LAM, Antignac A, Jéhanno M, et al. (2003) Nod1
819 Detects a Unique Muropeptide from Gram-Negative Bacterial Peptidoglycan.
820 Science 300: 1584-1587.
821 23. Arbibe L, Kim DW, Batsche E, Pedron T, Mateescu B, et al. (2007) An injected
822 bacterial effector targets chromatin access for transcription factor NF-[kappa]B to
823 alter transcription of host genes involved in immune responses. Nat Immunol 8: 47-
824 56.
825 24. Li H, Xu H, Zhou Y, Zhang J, Long C, et al. (2007) The Phosphothreonine Lyase
826 Activity of a Bacterial Type III Effector Family. Science 315: 1000-1003.

827 25. Kasper CA, Sorg I, Schmutz C, Tschon T, Wischnewski H, et al. (2010) Cell-Cell
828 Propagation of NF-κB Transcription Factor and MAP Kinase Activation Amplifies
829 Innate Immunity against Bacterial Infection. Immunity 33: 804-816.
830 26. Ray K, Marteyn B, Sansonetti PJ, Tang CM (2009) Life on the inside: the
831 intracellular lifestyle of cytosolic bacteria. Nat Rev Micro 7: 333-340.
832 27. Ashida H, Ogawa M, Kim M, Mimuro H, Sasakawa C (2012) Bacteria and host
833 interactions in the gut epithelial barrier. Nat Chem Biol 8: 36-45.
834 28. Pédron T, Thibault C, Sansonetti PJ (2003) The Invasive Phenotype of Shigella
835 flexneri Directs a Distinct Gene Expression Pattern in the Human Intestinal Epithelial
836 Cell Line Caco-2. J Biol Chem 278: 33878-33886.
837 29. CS F, DS M, C S-M, A D, AV R, et al. (2010) Microarray analysis of Shigella flexneri-
838 infected epithelial cells identifies host factors important for apoptosis inhibition. BMC
839 Genomics 11.
840 30. Stephen E. Girardin RT, Maria Mavris, Anne-Laure Page, Xiaoxia Li, George R.
841 Stark, John Bertin, Peter S. DiStefano, Moshe Yaniv, Philippe J. Sansonetti and
842 Dana J. Philpott (2001) CARD4/Nod1 mediates NF-κB and JNK activation by
843 invasive Shigella flexneri. EMBO Rep 2: 736–742.
844 31. Kim ML, Jeong HG, Kasper CA, Arrieumerlou C (2010) IKKα Contributes to
845 Canonical NF-κB Activation Downstream of Nod1-Mediated Peptidoglycan
846 Recognition. PLoS ONE 5: e15371.
847 32. Reiterer V, Grossniklaus L, Tschon T, Kasper CA, Sorg I, et al. (2011) Shigella
848 flexneri type III secreted effector OspF reveals new crosstalks of proinflammatory
849 signaling pathways during bacterial infection. Cell Signal 23: 1188-1196.

850 33. Tran Van Nhieu G, Enninga J, Sansonetti P, Grompone G (2005) Tyrosine kinase
851 signaling and type III effectors orchestrating Shigella invasion. Curr Opin Microbiol
852 8: 16-20.
853 34. Rogers LD, Brown NF, Fang Y, Pelech S, Foster LJ (2011) Phosphoproteomic
854 Analysis of Salmonella-Infected Cells Identifies Key Kinase Regulators and SopB-
855 Dependent Host Phosphorylation Events. Sci Signal 4: rs9-.
856 35. Bensimon A, Schmidt A, Ziv Y, Elkon R, Wang S-Y, et al. (2010) ATM-Dependent
857 and -Independent Dynamics of the Nuclear Phosphoproteome After DNA Damage.
858 Sci Signal 3: rs3-.
859 36. Huber A, Bodenmiller B, Uotila A, Stahl M, Wanka S, et al. (2009) Characterization
860 of the rapamycin-sensitive phosphoproteome reveals that Sch9 is a central
861 coordinator of protein synthesis. Genes Dev 23 1929-1943.
862 37. Olsen JV, Blagoev B, Gnad F, Macek B, Kumar C, et al. (2006) Global, In Vivo, and
863 Site-Specific Phosphorylation Dynamics in Signaling Networks. Cell 127: 635-648.
864 38. Schilling B, Rardin MJ, MacLean BX, Zawadzka AM, Frewen BE, et al. (2012)
865 Platform-independent and Label-free Quantitation of Proteomic Data Using MS1
866 Extracted Ion Chromatograms in Skyline. Molecular & Cellular Proteomics 11: 202-
867 214.
868 39. Schmidt A, Beck M, Malmstrom J, Lam H, Claassen M, et al. (2011) Absolute
869 quantification of microbial proteomes at different states by directed mass
870 spectrometry. Mol Syst Biol 7.
871 40. Glatter T, Ludwig C, Ahrné E, Aebersold R, Heck AJR, et al. (2012) Large-Scale
872 Quantitative Assessment of Different In-Solution Protein Digestion Protocols

873 Reveals Superior Cleavage Efficiency of Tandem Lys-C/Trypsin Proteolysis over
874 Trypsin Digestion. J Proteome Res 11: 5145-5156.
875 41. Köhler H RS, McCormick BA. (2002) Shigella flexneri Interactions with the
876 Basolateral Membrane Domain of Polarized Model Intestinal Epithelium: Role of
877 Lipopolysaccharide in Cell Invasion and in Activation of the Mitogen-Activated
878 Protein Kinase ERK. Infect Immun 70: 1150-1158.
879 42. Huang DW, Sherman BT, Lempicki RA (2008) Systematic and integrative analysis of
880 large gene lists using DAVID bioinformatics resources. Nat Protocols 4: 44-57.
881 43. Huang DW, Sherman BT, Lempicki RA (2009) Bioinformatics enrichment tools:
882 paths toward the comprehensive functional analysis of large gene lists. Nucleic
883 Acids Res 37: 1-13.
884 44. Nobes CD, Hall A (1995) Rho, Rac, and Cdc42 GTPases regulate the assembly of
885 multimolecular focal complexes associated with actin stress fibers, lamellipodia, and
886 filopodia. Cell 81: 53-62.
887 45. Ridley AJ HA (1992) Distinct patterns of actin organization regulated by the small
888 GTP-binding proteins Rac and Rho. Cold Spring Harb Symp Quant Biol 57: 10.
889 46. Sakaguchi T, Köhler H, Gu X, McCormick BA, Reinecker H-C (2002) Shigella
890 flexneri regulates tight junction-associated proteins in human intestinal epithelial
891 cells. Cell Microbiol 4: 367-381.
892 47. Iwai H, Kim M, Yoshikawa Y, Ashida H, Ogawa M, et al. (2007) A Bacterial Effector
893 Targets Mad2L2, an APC Inhibitor, to Modulate Host Cell Cycling. Cell 130: 611-
894 623.
895 48. Cao L YW, Wu Y, Yu L. (2009) The evolution, complex structures and function of
896 septin proteins. Cell Mol Life Sci 66: 3309-3323.

897 49. Mostowy S, Bonazzi M, Hamon MA, Tham TN, Mallet A, et al. (2010) Entrapment of
898 Intracytosolic Bacteria by Septin Cage-like Structures. Cell Host Microbe 8: 433-
899 444.
900 50. Mostowy S, Nam Tham T, Danckaert A, Guadagnini S, Boisson-Dupuis S, et al.
901 (2009) Septins Regulate Bacterial Entry into Host Cells. PLoS ONE 4: e4196.
902 51. Carneiro LAM, Travassos LH, Soares F, Tattoli I, Magalhaes JG, et al. (2009)
903 Shigella Induces Mitochondrial Dysfunction and Cell Death in Nonmyleoid Cells.
904 Cell Host Microbe 5: 123-136.
905 52. Szklarczyk D, Franceschini A, Kuhn M, Simonovic M, Roth A, et al. (2011) The
906 STRING database in 2011: functional interaction networks of proteins, globally
907 integrated and scored. Nucleic Acids Res 39: D561-D568.
908 53. Schwartz D, Gygi SP (2005) An iterative statistical approach to the identification of
909 protein phosphorylation motifs from large-scale data sets. Nat Biotech 23: 1391-
910 1398.
911 54. Manning G, Whyte DB, Martinez R, Hunter T, Sudarsanam S (2002) The Protein
912 Kinase Complement of the Human Genome. Science 298: 1912-1934.
913 55. Pendaries C, Tronchere H, Arbibe L, Mounier J, Gozani O, et al. (2006) PtdIns(5)P
914 activates the host cell PI3-kinase/Akt pathway during Shigella flexneri infection.
915 EMBO J 25: 1024-1034.
916 56. Uhlén M, Björling E, Agaton C, Szigyarto CA-K, Amini B, et al. (2005) A Human
917 Protein Atlas for Normal and Cancer Tissues Based on Antibody Proteomics.
918 Molecular & Cellular Proteomics 4: 1920-1932.
919 57. M. F (2005) Noise-Robust Soft Clustering Of Gene Expression Time-Course Data. J
920 Bioinform Comput Biol 3: 965–988.

921 58. Kim S-T, Lim D-S, Canman CE, Kastan MB (1999) Substrate Specificities and
922 Identification of Putative Substrates of ATM Kinase Family Members. J Biol Chem
923 274: 37538-37543.
924 59. O'Neill T, Dwyer AJ, Ziv Y, Chan DW, Lees-Miller SP, et al. (2000) Utilization of
925 Oriented Peptide Libraries to Identify Substrate Motifs Selected by ATM. J Biol
926 Chem 275: 22719-22727.
927 60. Kanehisa M, Goto S (2000) KEGG: Kyoto Encyclopedia of Genes and Genomes.
928 Nucleic Acids Res 28: 27-30.
929 61. Kanehisa M, Goto S, Sato Y, Furumichi M, Tanabe M (2012) KEGG for integration
930 and interpretation of large-scale molecular data sets. Nucleic Acids Res 40: D109-
931 D114.
932 62. Wullschleger S, Loewith R, Hall MN (2006) TOR Signaling in Growth and
933 Metabolism. Cell 124: 471-484.
934 63. Laplante M, Sabatini DM (2009) mTOR signaling at a glance. J Cell Sci 122: 3589-
935 3594.
936 64. Jacinto E, Loewith R, Schmidt A, Lin S, Ruegg MA, et al. (2004) Mammalian TOR
937 complex 2 controls the actin cytoskeleton and is rapamycin insensitive. Nat Cell Biol
938 6: 1122-1128.
939 65. Cybulski N, Zinzalla, V., & Hall, M. N. (2012) Inducible raptor and rictor Knockout
940 Mouse Embryonic Fibroblasts. Methods Mol Biol 821: 267-278
941 66. Magnuson B EB, Fingar DC. (2012) Regulation and function of ribosomal protein S6
942 kinase (S6K) within mTOR signalling networks. Biochem J 441: 1-21.

943 67. Knodler LA, Finlay BB, Steele-Mortimer O (2005) The Salmonella Effector Protein
944 SopB Protects Epithelial Cells from Apoptosis by Sustained Activation of Akt. J Biol
945 Chem 280: 9058-9064.
946 68. K N, VM D (2012) Signaling in innate immunity and inflammation. Cold Spring Harb
947 Perspect Biol
948 69. Chin AI, Dempsey PW, Bruhn K, Miller JF, Xu Y, et al. (2002) Involvement of
949 receptor-interacting protein 2 in innate and adaptive immune responses. Nature
950 416: 190-194.
951 70. Zhu Y, Li H, Long C, Hu L, Xu H, et al. (2007) Structural Insights into the Enzymatic
952 Mechanism of the Pathogenic MAPK Phosphothreonine Lyase. Molecular Cell 28:
953 899-913.
954 71. Burton EA, Oliver TN, Pendergast AM (2005) Abl Kinases Regulate Actin Comet Tail
955 Elongation via an N-WASP-Dependent Pathway. Mol Cell Biol 25: 8834-8843.
956 72. Liang Y, Hetzer MW (2011) Functional interactions between nucleoporins and
957 chromatin. Curr Opin Cell Biol 23: 65-70.
958 73. Bergounioux J, Elisee R, Prunier A-L, Donnadieu F, Sperandio B, et al. (2012)
959 Calpain Activation by the Shigella flexneri Effector VirA Regulates Key Steps in the
960 Formation and Life of the Bacterium's Epithelial Niche. Cell Host Microbe 11: 240-
961 252.
962 74. Ramel D, Lagarrigue F, Pons V, Mounier J, Dupuis-Coronas S, et al. (2011) Shigella
963 flexneri Infection Generates the Lipid PI5P to Alter Endocytosis and Prevent
964 Termination of EGFR Signaling. Sci Signal 4: ra61-.

965 75. Tattoli I, Sorbara MT, Vuckovic D, Ling A, Soares F, et al. (2012) Amino Acid
966 Starvation Induced by Invasive Bacterial Pathogens Triggers an Innate Host
967 Defense Program. Cell Host Microbe 11: 563-575.
968 76. Eyrich B, Sickmann A, Zahedi RP (2011) Catch me if you can: Mass spectrometry-
969 based phosphoproteomics and quantification strategies. Proteomics 11: 554-570.
970 77. Briggs MW, Sacks DB (2003) IQGAP proteins are integral components of
971 cytoskeletal regulation. EMBO Rep 4: 571-574.
972 78. Ohya K, Handa Y, Ogawa M, Suzuki M, Sasakawa C (2005) IpgB1 Is a Novel
973 Shigella Effector Protein Involved in Bacterial Invasion of Host Cells. J Biol Chem
974 280: 24022-24034.
975 79. Kim ML, Jeong HG, Kasper CA, Arrieumerlou C (2010) IKKalpha contributes to
976 canonical NF-kappaB activation downstream of Nod1-mediated peptidoglycan
977 recognition. PLoS One 5: e15371.
978 80. Carpenter A, Jones T, Lamprecht M, Clarke C, Kang I, et al. (2006) CellProfiler:
979 image analysis software for identifying and quantifying cell phenotypes. Genome
980 Biology 7: R100.
981 81. Perkins DN, Pappin DJC, Creasy DM, Cottrell JS (1999) Probability-based protein
982 identification by searching sequence databases using mass spectrometry data.
983 Electrophoresis 20: 3551-3567.
984 82. Smyth Gordon K (2004) Linear Models and Empirical Bayes Methods for Assessing
985 Differential Expression in Microarray Experiments. Stat Appl Genet Mol Biol.
986 83. Ting L, Cowley MJ, Hoon SL, Guilhaus M, Raftery MJ, et al. (2009) Normalization
987 and Statistical Analysis of Quantitative Proteomics Data Generated by Metabolic
988 Labeling. Mol Cell Proteomics 8: 2227-2242.

989 84. Vizcaíno JA, Côté RG, Csordas A, Dianes JA, Fabregat A, et al. (2013) The
990 Proteomics Identifications (PRIDE) database and associated tools: status in 2013.
991 Nucleic Acids Res 41: D1063-D1069.
992 85. Schindelin J, Arganda-Carreras I, Frise E, Kaynig V, Longair M, et al. (2012) Fiji: an
993 open-source platform for biological-image analysis. Nat Meth 9: 676-682.

994

995

FIGURE LEGENDS

Figure 1: Phosphoproteomics analysis applied to *S. flexneri* infection

(A) Diagram of the phosphoproteomics protocol applied to *S. flexneri* infection of HeLa cells. **(B)** Distribution of single, double, triple and quadruple peptide phosphorylation based on 3234 detected phosphopeptides (upper panel). Distribution of serine, threonine and tyrosine phosphorylation based on 3785 detected phospho-sites (lower panel). **(C)** Dynamics of phosphorylation changes after *S. flexneri* infection of HeLa cells. Data represent the number of phosphopeptides for which a significant increase (in blue) or a decrease (in red) of phosphorylation was observed after *S. flexneri* infection compared to uninfected cells. A minimum two-fold change and a q-value <0.01 were used to select phosphopeptides for quantification. **(D)** Dynamics of phosphorylation changes at the protein level after *S. flexneri* infection of HeLa cells. Data represent the number of proteins for which an increase of phosphorylation (in blue), a decrease of phosphorylation (in red) or both (in green) was observed after *S. flexneri* infection compared to uninfected cells. All proteins containing at least one phosphopeptide with a minimum two-fold change and a q-value <0.01 were considered for analysis.

Figure 2: Cellular processes affected by *S. flexneri*

(A) Gene ontology analysis of proteins with altered phosphorylation after *S. flexneri* infection performed with DAVID. All proteins (334) containing at least one phosphopeptide with a minimum two-fold change and a q-value <0.01 were considered for analysis (Phosphoproteome, in blue). As comparison, 334 randomly selected proteins containing at least one phosphopeptide with a ratio between 0.67 and 1.5 were

used as reference (Random selection, in red). Default *Homo sapiens* background was used for gene ontology analysis in DAVID. Full list of GO terms is shown in Table S3. (**B**) Literature-based manual annotation of the phosphoproteome. Numbers in brackets indicate the number of corresponding proteins. **(C)** Graphical representation of the phosphoproteome using STRING (high confidence 0.7) combined with manual functional annotation. Only proteins with at least one connection in STRING are represented.

Figure 3: Dynamics of phosphorylation changes after *S. flexneri* infection of epithelial cells.

(A) Dynamics of phosphorylation changes for individual phosphopeptides analyzed by fuzzy c-means clustering using the MFuzz algorithm. All individual phosphopeptides showing a significant change at least at one time-point were considered. Fold phosphorylation changes (log Ratio values) obtained for all time-points were normalized to have a standard deviation of 1 and a mean of 0 (z-score). For each cluster, the black line corresponds to an optimal membership of 1. The most overrepresented phospho-motif extracted with the motif-X algorithm was shown for each cluster. (**B**) Immunoblot of ATM phosphorylation at Ser-1981 in HeLa cells infected for the indicated time periods by *S. flexneri*. Vinculin was used as a loading control. **(C)** Densitometric quantification of ATM phosphorylation at Ser-1981 using the gel analysis tool from Fiji [85] (results representative of 2 independent experiments).

Figure 4: mTORC1 and mTORC2 control S6 kinase and AKT phosphorylation respectively

(A) Analysis of the most overrepresented KEGG signaling pathways of the phosphoproteome using DAVID. The dashed line indicates a negative log p-value threshold of 2. (**B**) Projection of mTOR-related proteins identified by phosphoproteomics onto an mTOR signaling map. (**C**) mTORC1 is required for S6 kinase and S6 ribosomal protein phosphorylation during *S. flexneri* infection. HeLa cells were left untreated or pretreated with rapamycin or PP242 for 60 minutes prior to *S. flexneri* infection (15 min) and analyzed by immunoblotting for the phosphorylation of S6 kinase at residue Thr-389 and of S6 ribosomal protein at Ser-235/236. Actin is used as a loading control. **(D)** The mTOR inhibitors rapamycin and PP242 do not affect *S. flexneri* entry. HeLa cells were pretreated either with rapamycin or PP242 at indicated concentrations for one hour, and infected with *S. flexneri* ΔvirG- pCK100 (P_{uhpT}::Dsred) for 3 hours. These bacteria, only fluorescent when they are intracellular, form large microcolonies that are effectively detected by automated image analysis. Quantification of the infection rate shows that inhibition of mTORC1 and mTORC2 fails to affect the entry process of *S. flexneri* into HeLa cells. Results are expressed as the mean ± SD corresponding to three different wells of a 96-well plate and are representative of two independent experiments. **(E)** *S. flexneri* infection-induced activation of AKT is mTORC2 dependent. HeLa cells were left untreated or pretreated with rapamycin or PP242 for 60 minutes prior to *S. flexneri* infection (15 min) and analyzed by immunobloting for the phosphorylation of AKT at Ser-473. Actin is used as a loading control. **(F)** mTORC2 component Rictor is required for the phosphorylation of AKT during *S. flexneri* infection. Control (Ctrl) and inducible-Rictor knockout (iRiKO) mouse embryonic fibroblasts were left untreated or infected with *S. flexneri* for 15 minutes and analyzed for the expression of Rictor and the level of AKT phosphorylation at Ser-473 by immunoblotting. Inducible Rictor-knockout was obtained

by tamoxifen pretreatment. AKT is used as loading control. All results were representative of at least two independent experiments.

Figure 5: *S. flexneri* and *S. typhimurium* infections trigger common host phosphorylation changes

(A) Venn diagram showing the overlap of phosphopeptides undergoing significant phosphorylation changes after *S. flexneri* infection (15 and 30 minutes) and *S. typhimurium* infection (10 and 20 minutes). For *S. typhimurium* infection, the phosphorylation events identified in different cellular compartments were compiled. **(B)** Phosphoproteins undergoing significant phosphorylation changes after both *S. flexneri* and *S. typhimurium* infections. Phosphoproteins were grouped according to different biological functions. Arrows indicate whether there is an increase or decrease in phosphorylation.

Figure 6: OspF has a wide –reaching impact on host protein phosphorylation

(A) OspF affects the phosphorylation of several signaling proteins involved in inflammation signaling. Left panels: OspF blocks the activation of p38 and ERK during *S. flexneri* infection. HeLa cells were left untreated or infected with either *S. flexneri* wild-type or Δ*ospF* for 30 minutes. The phosphorylation of p38 and ERK on residues T180/Y182 and T202/Y204 respectively, was analyzed by immunoblotting using the indicated phospho-specific antibodies. Right panels: OspF affects the phosphorylation of RIP2 and CREB on residue S176 and S133 respectively. Cells were left untreated or infected with *S. flexneri* wild-type or Δ*ospF* for 30 minutes. The phosphorylation of RIP2 and CREB was analyzed by immunoblotting using the indicated phospho-specific

antibodies. Actin was used as loading control (results representative of 2 independent experiments). **(B)** Hierarchical clustering analysis of relative peptide intensities obtained from the 3 independent replicates of cells infected for 30 minutes with either *S. flexneri* wild-type or Δo*spF.* Phosphopeptides showing a significant change between Δo*spF* and wild-type condition (two-fold change, q-value <0.01) were taken for the hierarchical clustering. **(C)** Graphical representation of the network of phosphoproteins affected by OspF (differential phosphoproteome). Phosphoproteins differentially phosphorylated between wild-type and Δ*ospF S. flexneri* were subjected to STRING (high confidence 0.7). Only proteins with at least one connection are represented. STRING data were combined to manual functional annotation. The known OspF targets p38 (MK14), ERK1 (MK03) and ERK2 (MK01) are highlighted by an increased node size. (**D**) Manual functional annotation of proteins from the differential phosphoproteome. Numbers in brackets indicate the number of corresponding proteins.

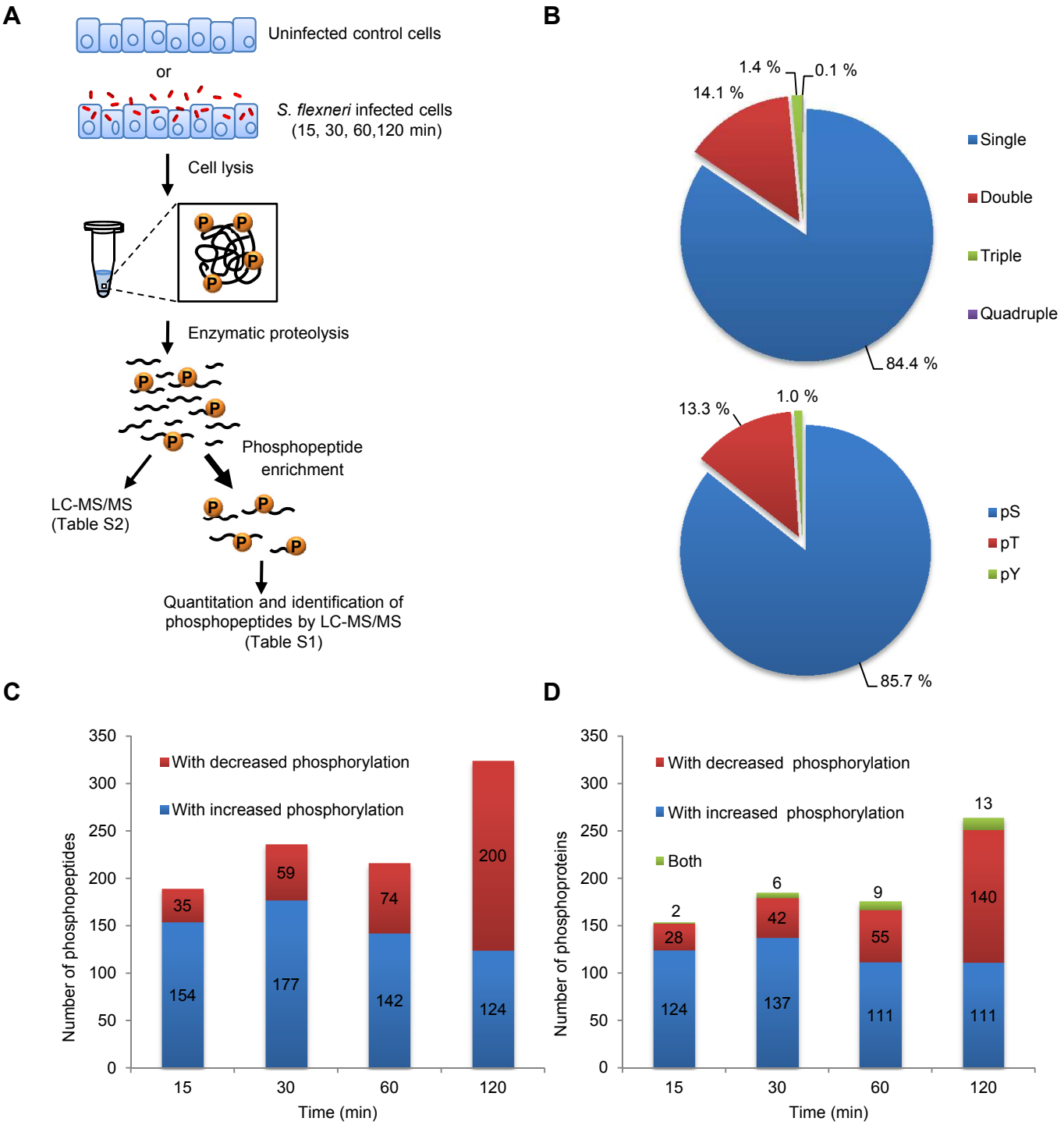
A
Uninfected control cells
or
S. flexneri infected cells
(15, 30, 60,120 min)
Cell lysis
Enzymatic proteolysis
Phosphopeptide
enrichment
LC-MS/MS
(Table S2)
Quantitation and identification of
phosphopeptides by LC-MS/MS
(Table S1)
B
1.4 %
0.1 %
14.1 %
84.4 %
Single
Double
Triple
Quadruple
13.3 %
1.0 %
85.7 %
pS
pT
pY
C
With decreased phosphorylation
With increased phosphorylation
Number of phosphopeptides
Time (min)
35
154
59
177
74
142
200
124
D
With decreased phosphorylation
With increased phosphorylation
Both
Number of phosphoproteins
Time (min)
2
28
124
6
42
137
9
55
111
13
140
111

Figure 1

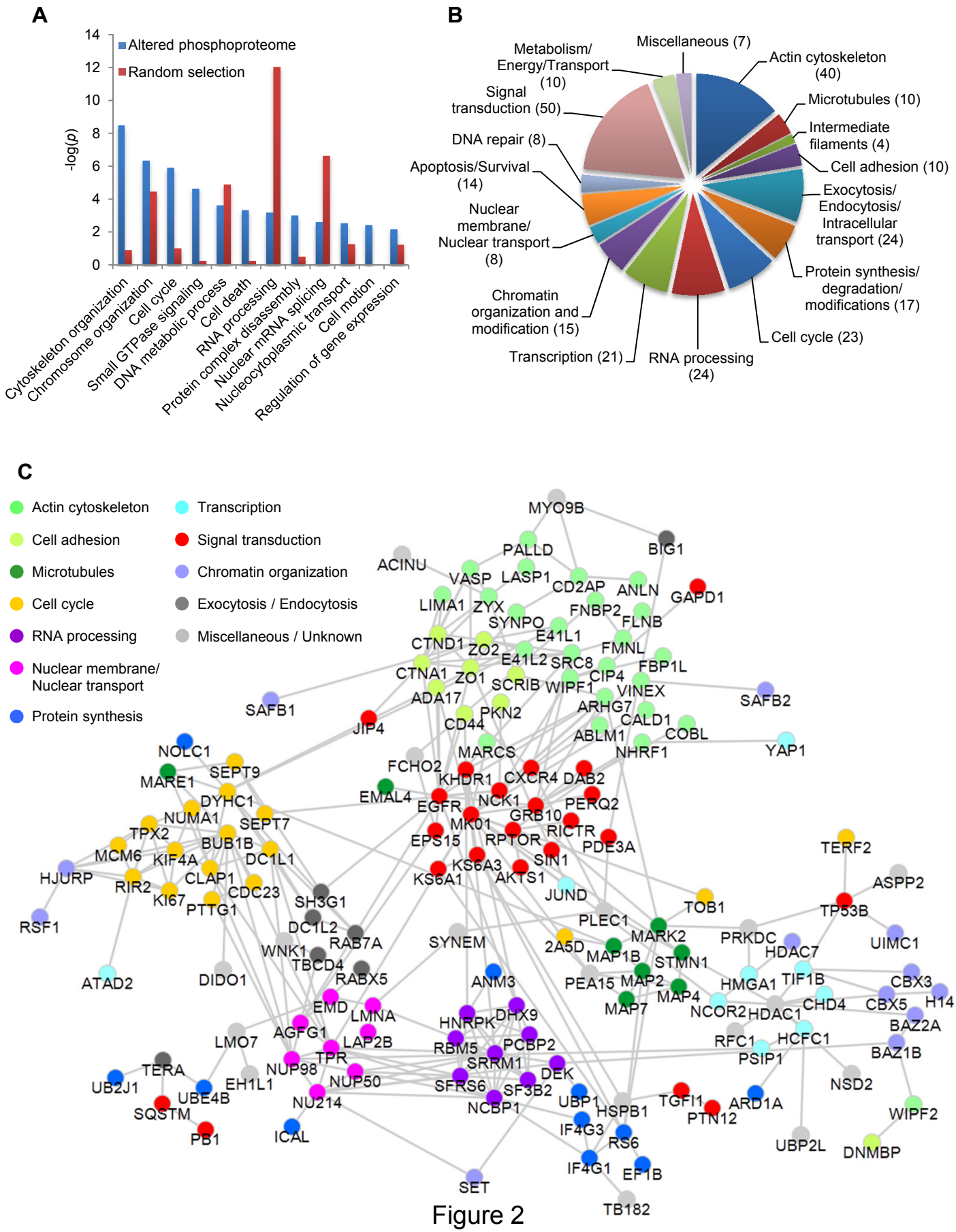
A
Altered phosphoproteome
Random selection
-log(p)
14
12
10
8
6
4
2
0
Cytoskeleton organization
Chromosome organization
Cell cycle
Small GTPase signaling
DNA metabolic process
Cell death
RNA processing
Protein complex disassembly
Nuclear mRNA splicing
Nucleocytoplasmic transport
Cell motion
Regulation of gene expression
B
Miscellaneous (7)
Actin cytoskeleton (40)
Microtubules (10)
Intermediate filaments (4)
Cell adhesion (10)
Exocytosis/ Endocytosis/ Intracellular transport (24)
Protein synthesis/ degradation/ modifications (17)
Cell cycle (23)
RNA processing (24)
Transcription (21)
Chromatin organization and modification (15)
Nuclear membrane/ Nuclear transport (8)
Apoptosis/Survival (14)
DNA repair (8)
Signal transduction (50)
Metabolism/ Energy/Transport (10)
C
Actin cytoskeleton
Cell adhesion
Microtubules
Cell cycle
RNA processing
Nuclear membrane/ Nuclear transport
Protein synthesis
Transcription
Signal transduction
Chromatin organization
Exocytosis / Endocytosis
Miscellaneous / Unknown
MYO9B
BIG1
ACINU
PALLD
VASP
LASP1
CD2AP
ANLN
GAPD1
LIMA1
ZYX
FNBP2
FLNB
SYNPO
E41L1
CTND1
ZO2
FMNL
E41L2
SRC8
FBP1L
CTNA1
ZO1
SCRIB
WIPF1
CIP4
VINEX
ADA17
PKN2
ARHG7
SAFB1
SAFB2
JIP4
CD44
CALD1
ABLM1
COBL
NOLC1
MARCS
NHRF1
YAP1
SEPT9
FCHO2
KHDR1
CXCR4
DAB2
MARE1
EMAL4
EGFR
NCK1
PERQ2
DYHC1
GRB10
NUMA1
MK01
RICTR
SEPT7
EPS15
RPTOR
PDE3A
TPX2
BUB1B
MCM6
KIF4A
DC1L1
KS6A3
SIN1
HJURP
CLAP1
KS6A1
AKTS1
RIR2
CDC23
KI67
PTTG1
SH3G1
JUND
TERF2
ASPP2
TOB1
TP53B
RSF1
DC1L2
PLEC1
RAB7A
MARK2
PRKDC
UIMC1
WNK1
SYNEM
2A5D
MAP1B
HDAC7
TBCD4
STMN1
ATAD2
DIDO1
RABX5
ANM3
PEA15
MAP2
HMGA1
TIF1B
CBX3
EMD
LMNA
MAP4
MAP7
NCOR2
HDAC1
CHD4
CBX5
H14
HNRPK
DHX9
BAZ2A
LMO7
AGFG1
LAP2B
RFC1
HCFC1
RBM5
PCBP2
PSIP1
BAZ1B
TERA
TPR
SRRM1
NUP98
DEK
NSD2
UB2J1
EH1L1
NUP50
SFRS6
SF3B2
UBP1
TGFI1
ARD1A
UBE4B
NU214
NCBP1
HSPB1
PTN12
WIPF2
SQSTM
IF4G3
UBP2L
PB1
ICAL
RS6
DNMBP
IF4G1
EF1B
SET
TB182

Figure 2

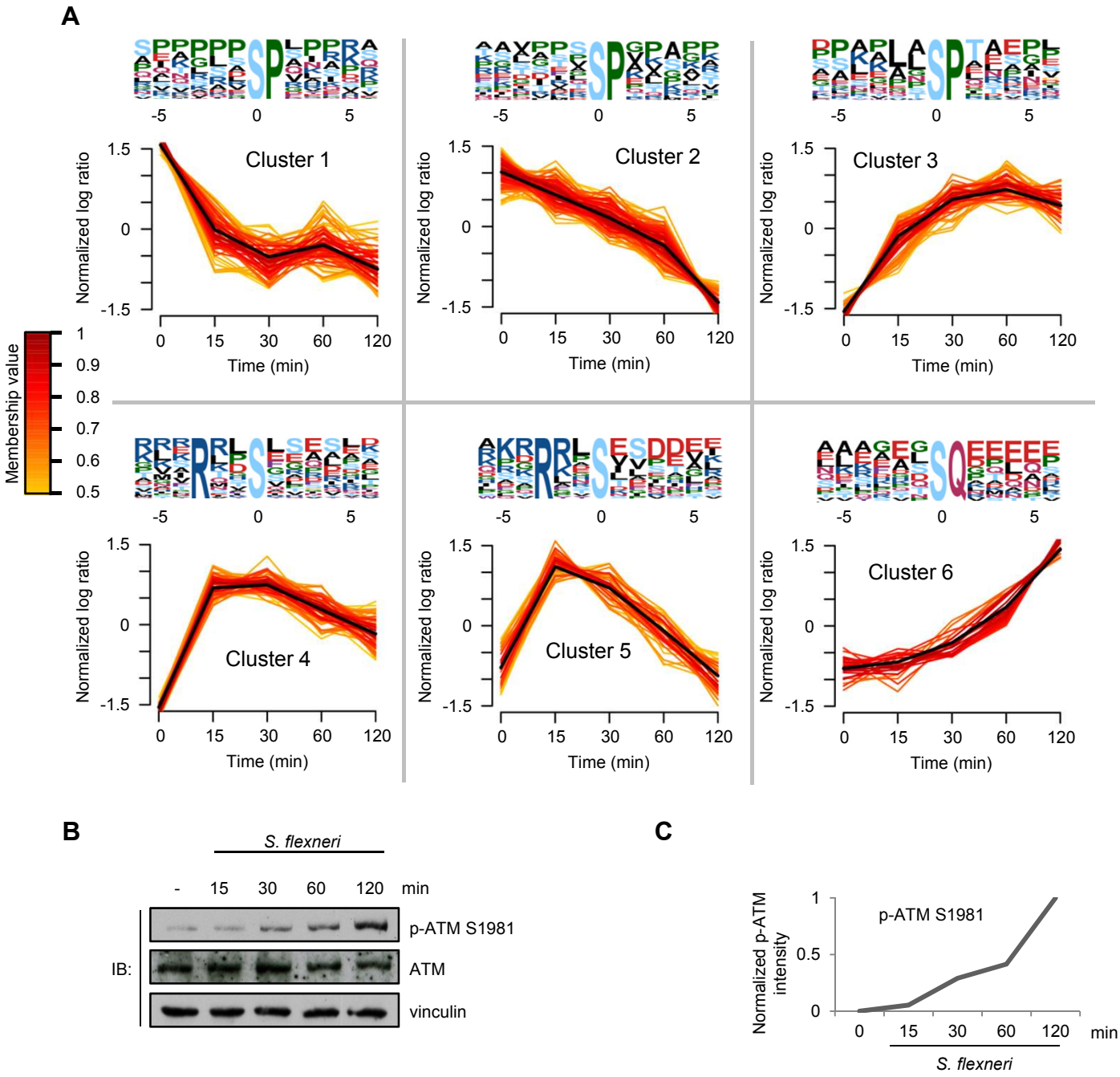
A
Cluster 1
Cluster 2
Cluster 3
Cluster 4
Cluster 5
Cluster 6
Normalized log ratio
Time (min)
Membership value
B
S. flexneri
- 15 30 60 120 min
IB:
p-ATM S1981
ATM
vinculin
C
p-ATM S1981
Normalized p-ATM intensity
min
S. flexneri

Figure 3

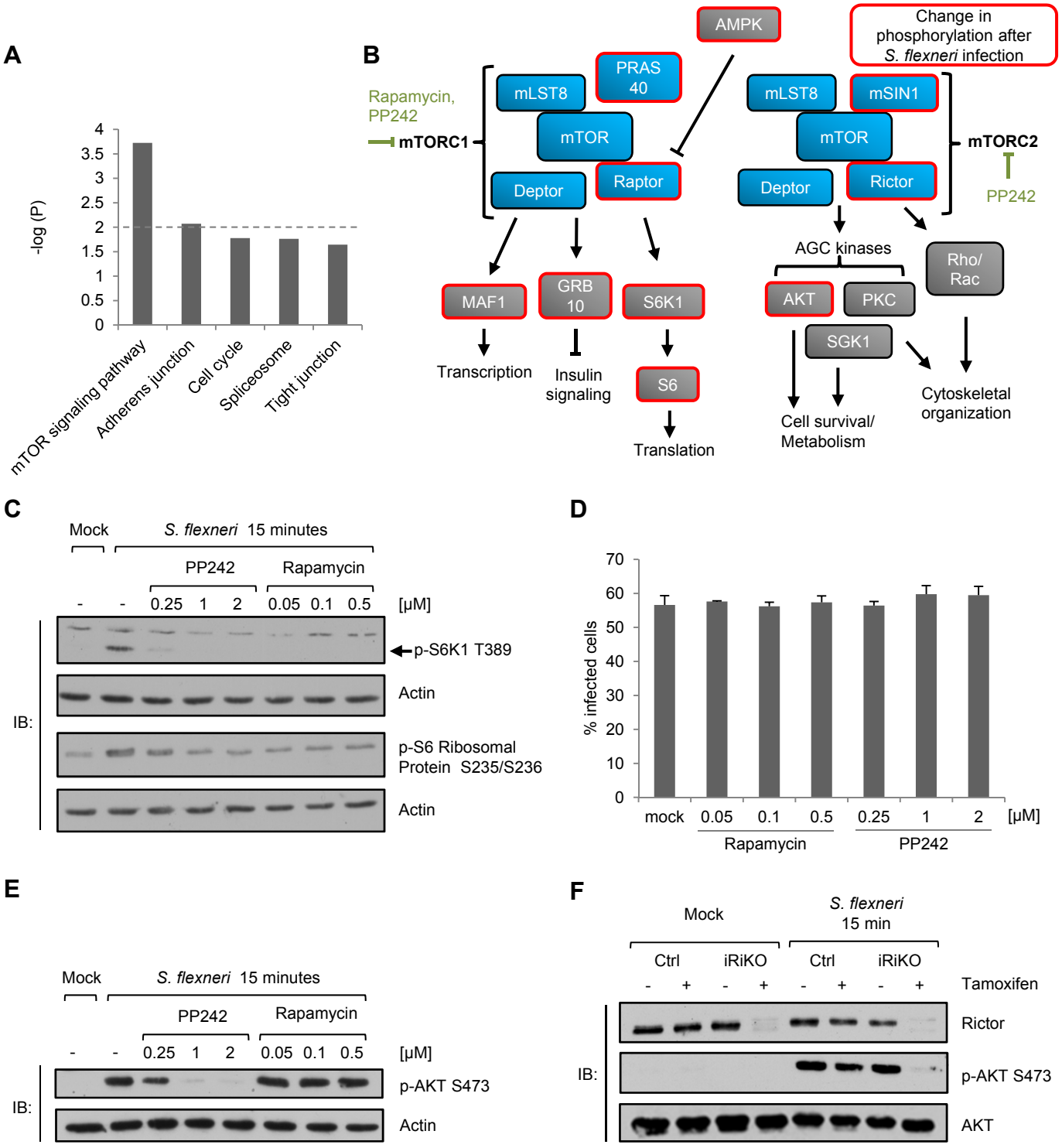
A
-log (P)
4
3.5
3
2.5
2
1.5
1
0.5
0
mTOR signaling pathway
Adherens junction
Cell cycle
Spliceosome
Tight junction
B
Rapamycin,
PP242
mTORC1
mLST8
PRAS
40
mTOR
Deptor
Raptor
AMPK
Change in
phosphorylation after
S. flexneri infection
mLST8
mSIN1
mTOR
Deptor
Rictor
mTORC2
PP242
MAF1
GRB
10
S6K1
Transcription
Insulin
signaling
S6
Translation
AGC kinases
AKT
PKC
Rho/
Rac
SGK1
Cell survival/
Metabolism
Cytoskeletal
organization
C
Mock
S. flexneri 15 minutes
PP242
Rapamycin
- - 0.25 1 2 0.05 0.1 0.5 [μM]
IB:
p-S6K1 T389
Actin
p-S6 Ribosomal
Protein S235/S236
Actin
D
% infected cells
70
60
50
40
30
20
10
0
mock 0.05 0.1 0.5 0.25 1 2 [μM]
Rapamycin
PP242
E
Mock
S. flexneri 15 minutes
PP242
Rapamycin
- - 0.25 1 2 0.05 0.1 0.5 [μM]
IB:
p-AKT S473
Actin
F
Mock
S. flexneri
15 min
Ctrl
iRiKO
Ctrl
iRiKO
- + - + - + - +
Tamoxifen
IB:
Rictor
p-AKT S473
AKT

Figure 4

A

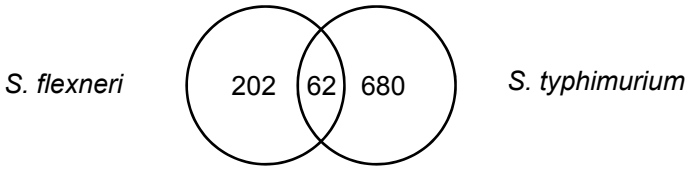

B

Protein ID	Protein Name	Phosphosites	Phosphorylation changes		Function
			S. flex.	*S. typhi.*	
TRIO	Triple functional domain protein	S2455/ S2459	↑	↑	Cytoskeleton
FMNL	Formin-like protein 1	S184	↓	↓	
IQGA2	Ras GTPase-activating-like protein	S16	↑	↑	
FBP1L	Formin-binding protein 1-like	S488	↑	↑	
PALLD	Palladin	S641/ S893	↑	↑	
CD2AP	CD2-associated protein	S458	↓	↓	
CTND1	Catenin delta-1	S252/ S268	↓	↓	
ZO1	Tight junction protein ZO-1	S617	↓	↓	
EPIPL	Epiplakin	S2691	↑	↑	
PLEC1	Plectin-1	S4626	↑	↑	
MAP1B	Microtubule-associated protein 1B	S2209/ S2211	↓	↓	
MAP7	Ensconsin	S365	↓	↓	
MYPT1	Protein phosphatase 1 regulatory subunit 12A	S507	↑	↑	
HSPB1	Heat shock protein beta-1	S15/ S82	↑	↑	
AHNK	Neuroblast differentiation-associated protein AHNAK	S210/ S5780/ S5784	↑	↑	Signaling
CXCR4	C-X-C chemokine receptor type 4	S324/ S325	↑	↑	
GAPD1	GTPase-activating protein and VPS9 domain-containing protein 1	S903	↑	↑	
TENS3	Tensin-3	S776	↑	↑	
PHIP	PH-interacting protein	S674	↑	↑	
AKP13	A-kinase anchor protein 13	S2567	↑	↑	
AKAP1	A kinase anchor protein 1, mitochondrial	S151	↑	↑	
APBB2	Amyloid beta A4 precursor protein-binding family B member 2	S123	↑	↑	
PB1	Protein polybromo-1	S39	↑	↑	
SH24A	SH2 domain-containing protein 4A	S315	↑	↑	
KIF4A	Chromosome-associated kinesin KIF4A	S801	↑	↑	Cell cycle
RIR2	Ribonucleoside-diphosphate reductase subunit M2	S20	↓	↓	
2A5D	Serine/threonine-protein phosphatase 2A regulatory subunit delta	S573	↑	↑	
BOD1L	Biorientation of chromosomes in cell division protein 1-like	S635	↑	↑	
SIPA1	Signal-induced proliferation-associated protein 1	S55	↑	↑	
SEPT9	Septin-9	S30	↑	↑	
DC1L1	Cytoplasmic dynein 1 light intermediate chain 1	T513/ T515	↑	↑	
BET1	BET1 homolog	S50	↑	↑	Transport
RAB7A	Ras-related protein Rab-7a	S72	↑	↑	
DEN4C	DENN domain-containing protein 4C	S1089	↑	↑	
GOGA5	Golgin subfamily A member 5	S116	↑	↑	
ACLY	ATP-citrate synthase	S455	↑	↑	Metabolism
S39A6	Zinc transporter ZIP6	S472	↑	↑	
NU214	Nuclear pore complex protein Nup214	S1023	↑	↑	Nuclear pore
NUP50	Nucleoporin 50 kDa	S221	↑	↑	
SNUT1	U4/U6.U5 tri-snRNP-associated protein 1	S448	↑	↑	Gene regulation
NCBP1	Nuclear cap-binding protein subunit 1	S22	↑	↑	
NUFP2	Nuclear fragile X mental retardation-interacting protein 2	S652	↑	↑	
PAIRB	Plasminogen activator inhibitor 1 RNA-binding protein	S330	↑	↑	
RBM14	RNA-binding protein 14	S618	↑	↑	
NELFE	Negative elongation factor E	S115	↑	↑	
HCFC1	Host cell factor	S666	↑	↑	
TR150	Thyroid hormone receptor-associated protein 3	S575	↑	↑	
PDCD4	Programmed cell death protein 4	S76/ S457	↑	↑	Miscellaneous/ Unknown
PRKRA	Interferon-inducible double stranded RNA-dependent protein kinase activator A	T20	↑	↑	
ZC11A	Zinc finger CCCH domain-containing protein 11A	S758	↑	↑	
FCHO2	FCH domain only protein 2	S387	↓	↓	
ZC3HD	Zinc finger CCCH domain-containing protein 13	S1014/ S1017	↓	↓	
PXDC2	Plexin domain-containing protein 2	S506	↑	↑	
EH1L1	EH domain-binding protein 1-like protein 1	S310	↑	↑	
TB182	182 kDa tankyrase-1-binding protein	S836	↑	↑	
K1522	Uncharacterized protein KIAA1522	S862	↓	↓	
CT2NL	CTTNBP2 N-terminal-like protein	T570	↓	↑	

Figure 5

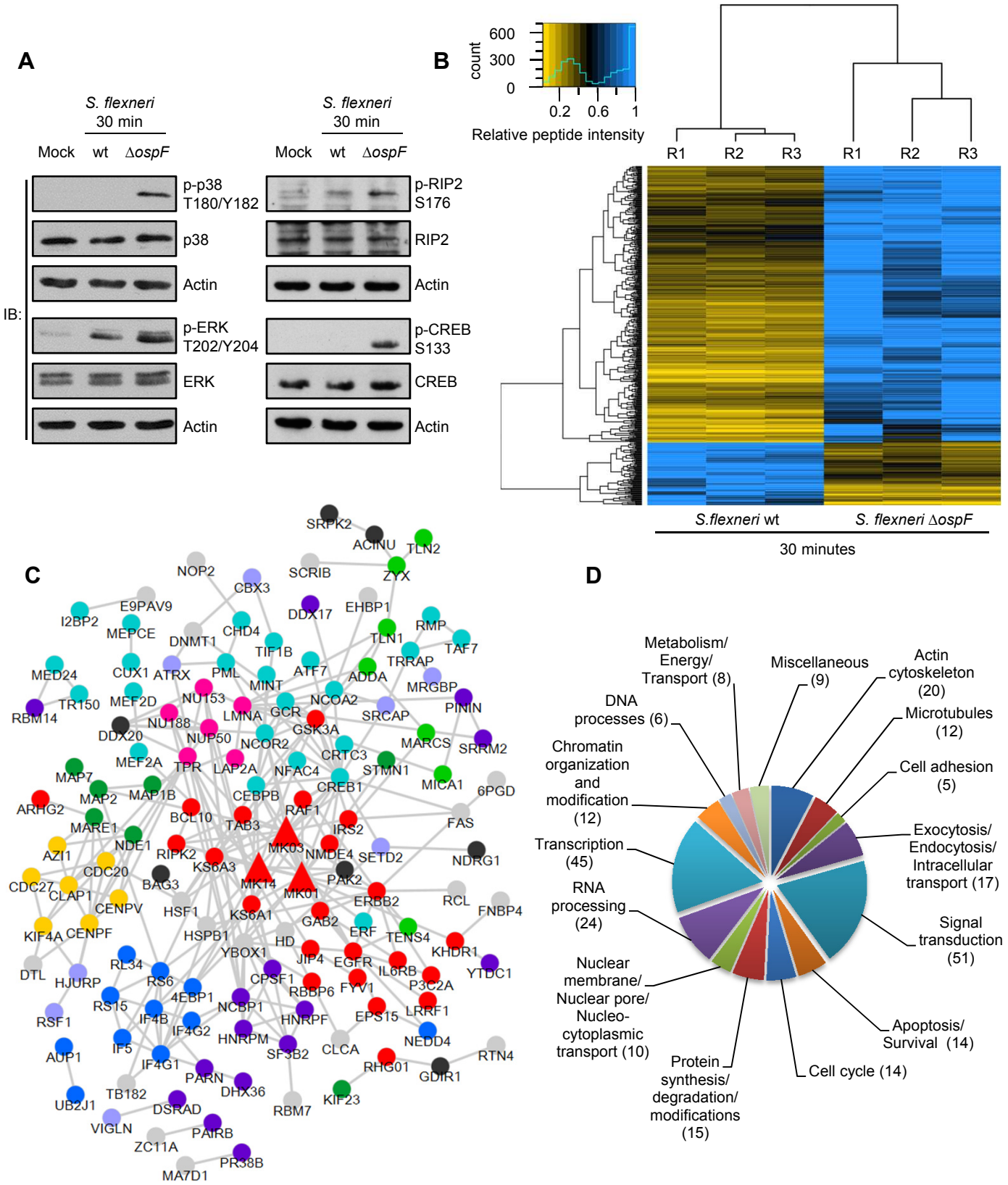
A
S. flexneri 30 min
Mock
wt
ΔospF
IB:
p-p38 T180/Y182
p38
Actin
p-ERK T202/Y204
ERK
Actin
p-RIP2 S176
RIP2
Actin
p-CREB S133
CREB
Actin
B
count
600
300
0
0.2
0.6
1
Relative peptide intensity
R1
R2
R3
R1
R2
R3
S.flexneri wt
S. flexneri ΔospF
30 minutes
C
SRPK2
ACINU
TLN2
NOP2
SCRIB
ZYX
CBX3
E9PAV9
I2BP2
MEPCE
DDX17
EHBP1
RMP
CHD4
DNMT1
TLN1
TAF7
TIF1B
TRRAP
MED24
CUX1
ATRX
PML
ATF7
ADDA
MRGBP
MINT
TR150
MEF2D
NU153
NCOA2
PININ
RBM14
LMNA
GCR
SRCAP
NU188
GSK3A
DDX20
NUP50
NCOR2
MARCS
SRRM2
CRTC3
MEF2A
TPR
LAP2A
NFAC4
STMN1
MAP7
MAP2
MAP1B
CEBPB
CREB1
MICA1
6PGD
ARHG2
BCL10
RAF1
MARE1
TAB3
IRS2
FAS
NDE1
AZI1
RIPK2
MK03
NMDE4
SETD2
NDRG1
KS6A3
CDC20
MK14
PAK2
CDC27
BAG3
MK01
CLAP1
ERBB2
RCL
FNBP4
CENPV
HSF1
KS6A1
GAB2
KIF4A
CENPF
HSPB1
ERF
TENS4
HD
KHDR1
YBOX1
JIP4
EGFR
IL6RB
YTDC1
DTL
HJURP
RL34
RS6
CPSF1
FYV1
P3C2A
RBBP6
4EBP1
RS15
NCBP1
EPS15
LRRF1
RSF1
IF4B
HNRPF
IF4G2
HNRPM
NEDD4
IF5
SF3B2
CLCA
RTN4
AUP1
IF4G1
RHG01
GDIR1
PARN
DHX36
TB182
KIF23
UB2J1
DSRAD
RBM7
VIGLN
PAIRB
ZC11A
PR38B
MA7D1
Microtubules
Actin cytoskeleton
Protein synthesis
RNA processing
Transcription
Signal transduction
Apoptosis
Cell Cycle
Chromatin organization/ modification
Nuclear membrane/ Nuclear transport
Miscellaneous / Unknown
D
Metabolism/ Energy/ Transport (8)
Miscellaneous (9)
Actin cytoskeleton (20)
DNA processes (6)
Microtubules (12)
Chromatin organization and modification (12)
Cell adhesion (5)
Transcription (45)
Exocytosis/ Endocytosis/ Intracellular transport (17)
RNA processing (24)
Signal transduction (51)
Nuclear membrane/ Nuclear pore/ Nucleo-cytoplasmic transport (10)
Apoptosis/ Survival (14)
Protein synthesis/ degradation/ modifications (15)
Cell cycle (14)

Figure 6